

# Internship Report

Search of potential atmospheres on the external  
planets of the TRAPPIST-1 system from previous  
JWST observations

Louis-Julien Cartigny

M1 Sciences de l'Univers et Technologies Spatiales  
Observatoire de Paris - PSL

Supervisors: Alice Maurel & Elsa Ducrot

January - June 2025

Institut d'Astrophysique de Paris, UMR 7095  
Laboratoire d'Instrumentation et de Recherche en Astrophysique, UMR 8254



 Observatoire  
de Paris | PSL★

---

## Abstract

**Context:** In 2016 and 2017, seven Earth-sized planets were discovered around the nearby M-type star TRAPPIST-1 with several of them in the habitable zone, making this system a very interesting target for the study of habitability. Recent observations suggest that the two innermost planets are probably bare rocks without any atmosphere. However, it is not possible to replicate these studies with the five outer planets as they are too cool.

**Aims:** I tried to estimate the contribution of the outer planets to observed fluxes from previous JWST observations in the two extreme cases of all bare rocks and of all planets with thick atmospheres to determine whether the difference is detectable by the JWST.

**Methods:** I wrote a Python code to simulate the phase curves of each of the seven planets of TRAPPIST-1 and estimate the flux contribution of the outer planets, either in absolute flux or in relative flux. I compared these simulations with JWST fluxes from previous studies and with previous JWST data I analyzed using the Eureka! pipeline.

**Results:** The previous JWST data in absolute fluxes have too large error bars to determine whether the outer planets are all bare rocks or all have thick atmospheres. However, the amplitude of the simulated variations in relative flux could be detected by the JWST, provided that the observation is long enough to measure the whole variation of the total flux from the outer planets.

**Key words:** Exoplanet - TRAPPIST-1 - Phase curve - Atmosphere - JWST - MIRI

## Contents

<b>1</b>	<b>Introduction</b>	<b>4</b>
<b>2</b>	<b>Methodology</b>	<b>5</b>
2.1	Study of transiting exoplanets . . . . .	5
2.1.1	Orbital parameters . . . . .	5
2.1.2	Transit and eclipse parameters . . . . .	6
2.1.3	Emitted fluxes . . . . .	8
2.1.4	Phase curves . . . . .	10
2.1.5	Transit timing variations . . . . .	11
2.1.6	Overview of the TRAPPIST-1 system . . . . .	12
2.2	Simulation of phase curves using Python . . . . .	13
2.2.1	Working hypotheses . . . . .	13
2.2.2	Code overview . . . . .	15
2.3	Analysis of JWST data . . . . .	16
2.3.1	Dataset and instrument used . . . . .	16
2.3.2	The Eureka! pipeline . . . . .	17
2.3.3	Bayesian inference and MCMC . . . . .	18
<b>3</b>	<b>Results</b>	<b>20</b>
3.1	Simulation of fluxes and phase curves . . . . .	20
3.1.1	General check with the bolometric fluxes . . . . .	20
3.1.2	Simulations of the JWST observations . . . . .	21
3.2	Data from JWST observations . . . . .	21
3.2.1	Analysis with Eureka! . . . . .	21
3.3	Comparisons . . . . .	27
3.3.1	Stellar fluxes comparisons . . . . .	27
3.3.2	Placement of JWST observations over the simulated phase curves . . . . .	27
<b>4</b>	<b>Conclusion and perspectives</b>	<b>29</b>
	<b>Acknowledgments</b>	<b>31</b>
	<b>References</b>	<b>32</b>
<b>A</b>	<b>Appendix: Additional figures</b>	<b>34</b>
<b>B</b>	<b>Appendix: Presentation of the Exoplanets_Phase_Curves codes</b>	<b>37</b>
<b>C</b>	<b>Appendix: Observations with JWST</b>	<b>38</b>

## 1 Introduction

The discovery of 51-Pegasi b by [Mayor and Queloz \(1995\)](#), the first exoplanet detected around a main-sequence star, initiated a whole new field of astronomy: exoplanetology. Since then, almost 6,000 exoplanets have been detected, with several thousands more yet to be confirmed, according to the NASA Exoplanet Archive website. Nevertheless, for two decades exoplanetology consisted mainly in detecting giant planets with short orbital periods. Indeed, there is an observational bias due to the two main techniques used to detect exoplanets: the radial velocities and the transit methods. The former, used by [Mayor and Queloz \(1995\)](#) to detect 51-Pegasi b, consists of measuring the Doppler shift in the light from a star due to its motion caused by the gravitational attraction of a planet orbiting it, while the latter consists of detecting the drop of light from the star when it is partially blocked by an exoplanet passing between it and the observer. These two methods thus favor the study of big planets near the size of Jupiter with very short orbital periods of only a few days which have been called hot-Jupiters.

However, the James Webb Space Telescope (JWST) ([Gardner et al. 2023](#)), launched in December 2021, permitted to start characterizing their atmospheres, not only for the hot-Jupiters but also for Earth-sized planets orbiting cool stars.

Indeed, as cool stars are much smaller than Solar-like stars, they make perfect targets for the study of transiting rocky planets. As the depth of a transit depends on the ratio of the planetary and stellar radii squared, the ones of Earth-sized planets around cool stars barely bigger than Jupiter can easily be characterized by the JWST.

It was in this scope that the JWST performed several observations in the mid-infrared of the two innermost planets of the TRAPPIST-1 system ([Gillon et al. 2016](#)). This system, at only 40 light years from the Solar System, is composed of seven Earth-sized transiting planets orbiting an M8-type star with short orbital periods from 1.5 to 18 days. Three of these planets are in the habitable zone, which makes this system a very interesting target not only for exoplanetology but also for the understanding of habitability. Several studies suggested that probably neither TRAPPIST-1 b ([Ducrot et al. 2024b](#)) or c ([Zieba et al. 2023](#)), the two planets that are the closest to the star, have any substantial atmosphere. However, due to their longer orbital periods, it is not possible to perform the same kind of study in emission for the five outer planets as they receive far less light from the star and thus are colder and as it would require far too much observation time from the JWST.

To do so, we can instead analyze the total signal from the system in thermal emission and determine, using simulations, which parts of it are due to the contribution of the outer planets. During my M1 internship at the Institut d'Astrophysique de Paris (IAP) and at the Laboratoire d'Instrumentation et de Recherche en Astrophysique (LIRA) of Paris' Observatory, supervised by Alice Maurel (IAP/LMD) and Elsa Ducrot (LIRA/CEA), I modeled the phase curves of the seven planets of the TRAPPIST-1 system and compared them with JWST data considering two different cases: 1) that the outer planets are bare rocks with no atmosphere at all or 2) that they have a thick atmosphere allowing a global temperature redistribution. My objective was to determine whether the flux difference between these two models was important enough to be detected in the JWST Mid-Infrared Instrument (MIRI) ([Rieke et al. 2015](#)) data from observations of TRAPPIST-1 b and c performed between October 2022 and December 2024.

In this report, I will first go through the theoretical elements about the study of transiting exoplanets that I used during my internship to write my `Exoplanets_Phase_Curves` codes in Python and introduce the TRAPPIST-1 planetary system. Then, I will present my strategy to simulate the phase curves of the planets and an overview of the `Exoplanet_Phase_Curves` codes before introducing the instrument, datasets and the Eureka! Python pipeline I used to perform analyses of JWST data. Finally, I will go through the results of my simulations and of the data analysis and of the comparison between the two.

## 2 Methodology

### 2.1 Study of transiting exoplanets

There are many ways to study exoplanets, however here we will mainly focus on transiting planets, like the planets of TRAPPIST-1, and pay attention in particular to their secondary eclipses. The transit method consists in detecting the drop of luminosity from the star when a planet passes in front of it. Of course, this method of detection requires that the planet have an orbit such that it passes between its star and the observer. In this section, I will go through all the theoretical elements that I needed to write my Exoplanet\_Phase\_Curve codes to simulate the phase curves in emitted light of the TRAPPIST-1 planets.

#### 2.1.1 Orbital parameters

As for the planets of the Solar System, the orbit of an exoplanet is ruled by the three Kepler laws and is characterized in three dimensions by several parameters (see Figure 1) :

- $a$ , the semi-major axis, and  $P$ , the orbital period, which are linked to each other by Kepler's third law :  $\frac{a^3}{P^2} = \frac{GM}{4\pi^2}$  (with  $G$  the gravitational constant and  $M$  the mass of the star);
- $e$ , the eccentricity (if  $e = 0$ , then the orbit is circular);
- $i$ , the orbit's inclination with respect to a reference plane which corresponds to the sky plane for exoplanets (for a transiting exoplanet  $i$  is thus near  $90^\circ$ );
- $t_P$ , a reference time for which the position of the planet on its orbit is known (it usually corresponds to a passage at the pericentre);
- $\Omega$ , the longitude of the ascending node, i.e the point where the orbit crosses the reference plane while the planet is moving away the observer (in the  $z$  direction in Figure 1);
- $\omega$ , the argument of periastron, i.e the angular coordinate of the planet's pericentre relatively to the ascending node  $\Omega$ .

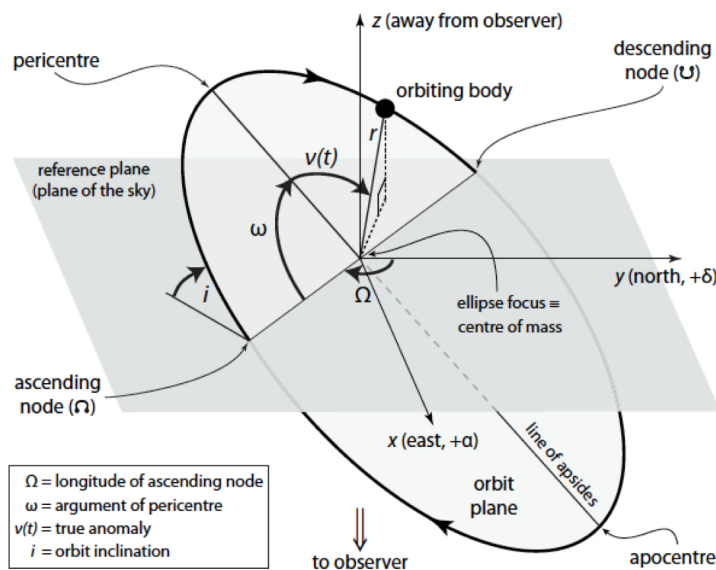


Figure 1: View of an elliptical orbit in three dimensions (Figure from Perryman (2018))

The distance of the planet from its star (also called star-planet separation) at a given time can be determined by using the following equation:

$$r = \frac{a(1 - e^2)}{1 + e \cos \nu} \quad (1)$$

where  $\nu$  is the planet's true anomaly, i.e the angle between the directions of the pericenter and of its current position measured at the barycentric focus  $F_1$  of the ellipse (see Figure 2).

The true anomaly can be computed using the mean anomaly  $M(t)$ , a fictitious angle related to the mean motion of the planet  $n = \frac{2\pi}{P}$ , which is defined as  $M(t) = (t - t_P)n$ .

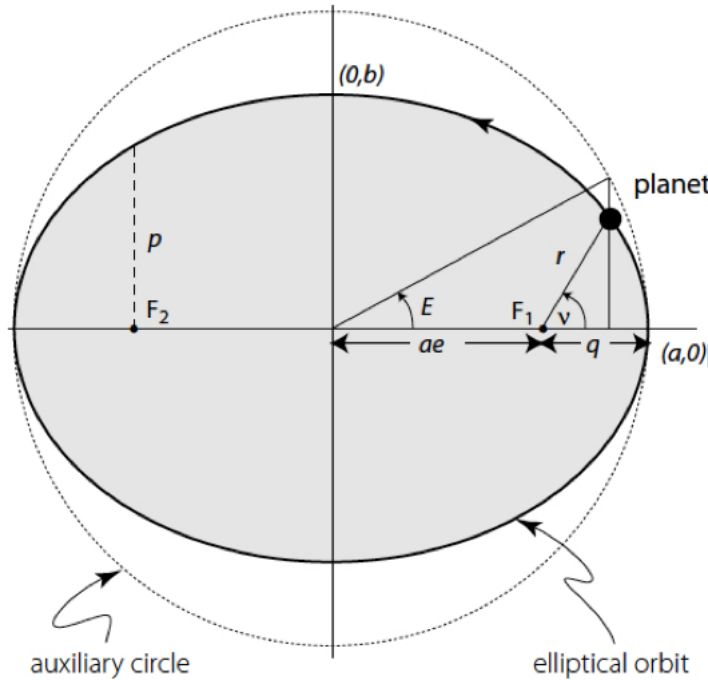


Figure 2: View of an elliptical orbit in two dimensions (Figure from [Perryman \(2018\)](#))

As shown in Figure 2, we can also describe the position of a planet on its orbit in terms of eccentric anomaly  $E$ , i.e with respect to an auxiliary circle of radius equal to the ellipse's semi-major axis  $a$ , which is related to the true anomaly  $\nu$  by:

$$\cos \nu(t) = \frac{\cos E(t) - e}{1 - e \cos E(t)} \quad (2)$$

The mean and eccentric anomalies are related by Kepler's equation:

$$M(t) = E(t) - e \sin E(t) \quad (3)$$

### 2.1.2 Transit and eclipse parameters

When an exoplanet with an inclination near  $90^\circ$  and its host star are at conjunction (i.e when the two bodies are nearly aligned on the observer's line of sight), it leads to two phenomena: primary eclipses, also called transits, and secondary eclipses, also called occultations or just eclipses. As shown in Figure 3, transits occur when the exoplanet passes in front of its star, causing a drop of the observed flux, while eclipses occur when the planet passes behind its star, also causing a shallower drop of the flux.

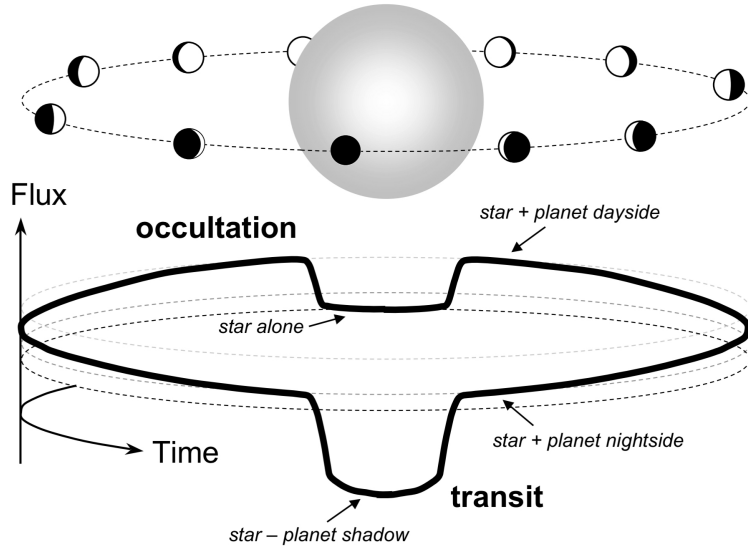


Figure 3: Illustration of a transit and an eclipse with the evolution of the star+planet flux along the planet's orbit (Figure from [Winn \(2014\)](#))

These two phenomena can be described using several parameters. First, the impact parameter  $b$  represents the projected distance at conjunction between the star and planet centers in units of stellar radius:

$$b = \frac{a \cos i}{R_{star}} \left( \frac{1 - e^2}{1 \pm e \sin \omega} \right) \quad (4)$$

with:

- $a$ , the planet's semi-major axis;
- $i$ , its orbital inclination;
- $R_{star}$ , the stellar radius;
- $e$ , the planet's orbital eccentricity;
- $\omega$ , the argument of periastron.

The  $\pm$  refers to a transit when set to a  $+$  and to an eclipse when set to a  $-$ .

The transit depth  $\Delta F = \delta \approx \left( \frac{R_{planet}}{R_{star}} \right)^2$  corresponds to the fraction of light from the star that is blocked by the planet during the transit.

In addition, as explained by [Winn \(2014\)](#) and illustrated in Figure 4, the total transit duration  $T_{total} = t_{IV} - t_I$  is the lapse of time between the fourth and first contact times while the full transit duration  $T_{full} = t_{III} - t_{II}$  is the one between the third and second contact times. The duration between the second and first contact  $\tau_{ingress} = t_{II} - t_I$  is called the ingress duration and the one between the fourth and third contact times  $\tau_{regress} = t_{IV} - t_{III}$  is called the egress duration. As shown in Figure 4, the four contact times  $t_{I-IV}$  correspond to the times at which the stellar and planetary disks are tangent.

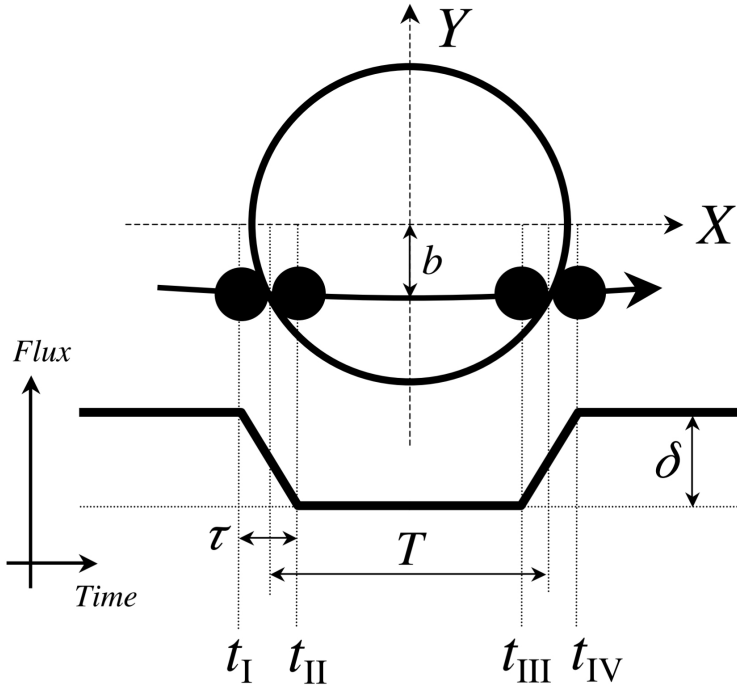


Figure 4: Illustration of the different transit parameters (Figure from Winn (2014))

An other way to express the total and full transit and eclipse durations is:

$$T_{total} = t_{IV} - t_I = \frac{P}{\pi} \sin^{-1} \left[ \frac{\sqrt{(1 + R_{planet}/R_{star})^2 - b^2}}{1 - \cos^2 i} \right] \frac{\sqrt{1 - e^2}}{1 \pm e \sin \omega} \quad (5)$$

$$T_{full} = t_{III} - t_{II} = \frac{P}{\pi} \sin^{-1} \left[ \frac{\sqrt{(1 - R_{planet}/R_{star})^2 - b^2}}{1 - \cos^2 i} \right] \frac{\sqrt{1 - e^2}}{1 \pm e \sin \omega} \quad (6)$$

with:

- $P$ , the planet's orbital period;
- $R_{planet}$ , the planetary radius;
- $R_{star}$ , the stellar radius;
- $b$ , the impact parameter (see Eq. 4);
- $i$ , the planet's orbital inclination;
- $e$ , its orbital eccentricity;
- $\omega$ , the argument of periastron.

As for Eq. 4, the  $\pm$  refers to a transit when set to a  $+$  and to an eclipse when set to a  $-$ .

### 2.1.3 Emitted fluxes

The planets of the TRAPPIST-1 system can all be approximated as black bodies. Thus, their spectral radiance  $\mathcal{B}_\lambda(T)$  in  $\text{W}\cdot\text{m}^{-2}\cdot\text{m}^{-1}\cdot\text{sr}^{-1}$  is given by the Planck's law:

$$\mathcal{B}_\lambda(T) = \frac{2hc^2\lambda^{-5}}{e^{\frac{hc}{\lambda kT}} - 1} \quad (7)$$

with:

- $\lambda$ , the wavelength in m;
- $h \approx 6.626 \cdot 10^{-34}$  J·s, the Planck constant;
- $c = 2.99792458 \cdot 10^8$  m/s, the speed of light in vacuum;
- $k \approx 1.38 \cdot 10^{23}$  J·K<sup>-1</sup>, the Boltzmann constant.

As explained by [Ducrot \(2021\)](#), we can model the temperature of the day side and the night side of a tidally locked exoplanet by using the formalism of [Cowan and Agol \(2010\)](#), which quantifies the thermal redistribution efficiency:

$$\begin{aligned} T_{\text{day side}} &= T_{\text{star}} \sqrt{\frac{R_{\text{star}}}{d}} \left[ (1 - A_B) \left( \frac{2}{3} - \epsilon \frac{5}{12} \right) \right]^{1/4}, \\ T_{\text{night side}} &= T_{\text{star}} \sqrt{\frac{R_{\text{star}}}{d}} \left[ (1 - A_B) \left( \frac{\epsilon}{4} \right) \right]^{1/4}, \end{aligned} \quad (8)$$

with:

- $T_{\text{star}}$ , the effective temperature of the star in K;
- $R_{\text{star}}$ , the stellar radius in m;
- $d = r = \frac{a(1-e^2)}{1+e \cos \nu}$ , the star-planet separation (see Eq. 1);
- $A_B$ , the Bond albedo of the planet, i.e its capacity to reflect the light from its star (comprised between 0 and 1);
- $\epsilon$ , the efficiency of the thermal redistribution between the day side and the night side (also comprised between 0 and 1).

In the case of a full redistribution, i.e when  $\epsilon = 1$ , we can notice that the temperature is homogeneous all over the planet with  $T_{\text{day side}} = T_{\text{night side}}$ . The planets re-emits one fourth of the flux it receives from the star. On the opposite, when we have no day-night redistribution at all,  $\epsilon = 0$ , the day side of the planet re-emits two thirds of the flux it receives from the star while the temperature of the night side is null.

It is also important to point out that the factor  $T_{\text{star}} \sqrt{\frac{R_{\text{star}}}{d}}$  in Eq. 8 corresponds to the temperature of the substellar point, i.e the point of the planet day side on which the light rays from the star are perpendicular to the surface.

To compute the ratio of emitted flux between the planet and the star in a given spectral range  $[\lambda_1, \lambda_2]$ , we need to take into account the ratio of their radii and integrate their spectral radiance  $\mathcal{B}_\lambda(T)$  over that spectral range:

$$\frac{F_{\text{planet}}}{F_{\text{star}}} = \left( \frac{R_{\text{planet}}}{R_{\text{star}}} \right)^2 \frac{\int_{\lambda_1}^{\lambda_2} \mathcal{B}_\lambda(T_{\text{planet}}) d\lambda}{\int_{\lambda_1}^{\lambda_2} \mathcal{B}_\lambda(T_{\text{star}}) d\lambda} \quad (9)$$

with:

- $R_{\text{planet}}$ , the planetary radius in m;
- $R_{\text{star}}$ , the stellar radius in m;
- $T_{\text{planet}}$ , the equilibrium temperature of the planet in K;
- $T_{\text{star}}$ , the effective temperature of the star in K.

I first worked with bolometric fluxes, i.e over all wavelengths, as a first approximation to qualitatively simulate the phase curves (see Section 2.1.4). In that case, the flux of the star (in  $\text{W/m}^2$ ) received at distance  $d$  can be expressed using its luminosity  $L_{\text{star}}$ :

$$F_{\text{star}} = \frac{L_{\text{star}}}{4\pi d^2} \quad (10)$$

As explained in Eq. 8, the re-emitted flux of a tidally locked planet with no thermal redistribution is equal to two thirds of the one it receives from its star:  $F_{\text{planet}} = \frac{2}{3}F_{\text{received}}$ . Thus, the luminosity of the planet day side is:

$$L_{\text{dayside}} = \frac{1}{2}F_{\text{planet}} 4\pi R_{\text{planet}}^2 \quad (11)$$

So, the bolometric flux ratio between the planet and the star is:

$$\frac{F_{\text{planet}}}{F_{\text{star}}} = \frac{L_{\text{planet}}}{L_{\text{star}}} \left( \frac{R_{\text{planet}}}{R_{\text{star}}} \right)^2 \quad (12)$$

#### 2.1.4 Phase curves

It is also possible to study a planet outside of a transit or an eclipse by measuring the planet's flux all along its orbit for different phases. There are several ways to describe the phase of a planet, so here I will only present the ones that I used in my codes. A general one is to define it as a phase angle  $\alpha$  as explained by [Perryman \(2018\)](#):

$$\cos \alpha = \sin(\omega + \nu) \sin i \quad (13)$$

with:

- $\omega$ , the planet's argument of periastron;
- $\nu$ , its true anomaly;
- $i$ , its orbital inclination.

There are also several ways of defining how the phase varies along the planet's orbit, which is called a phase function. One of them is by considering the planet as a Lambert sphere scattering the light isotropically over  $2\pi$  sr ([Agol 2007](#)):

$$g(\alpha) = \frac{\sin \alpha + (\pi - \alpha) \cos \alpha}{\pi} \quad (14)$$

However, for transiting planets on a circular orbit with a low inclination, it is possible to define the phase in a more simple way as the ratio of the elapsed time  $t$  since the planet's last transit over its orbital period  $P$ :  $\frac{t}{P}$ . At mid-transit the phase would then be equal to 0 or 1 and to 0.5 at mid-eclipse. The phase function can also be simplified as a sinusoidal variation between 0 at mid-transit and 1 at mid-eclipse:

$$g(t) = \frac{1}{2} \sin \left( \frac{t - t_{\text{transit}}}{P} 2\pi \right) + 0.5 \quad (15)$$

with  $t_{\text{transit}}$  the time of a known transit. As shown in Figure 5, the maxima of this model are less peaked than the Lambertian one. However, what really interests us is the amplitude between the maxima and minima and the period of the signal, which is the same for both models. The drops to zero at each maximum correspond to the eclipses during which the emitted planetary flux is completely hidden by the star. The transits on the other hand occur at the minima, i.e when the planet presents only its night side.

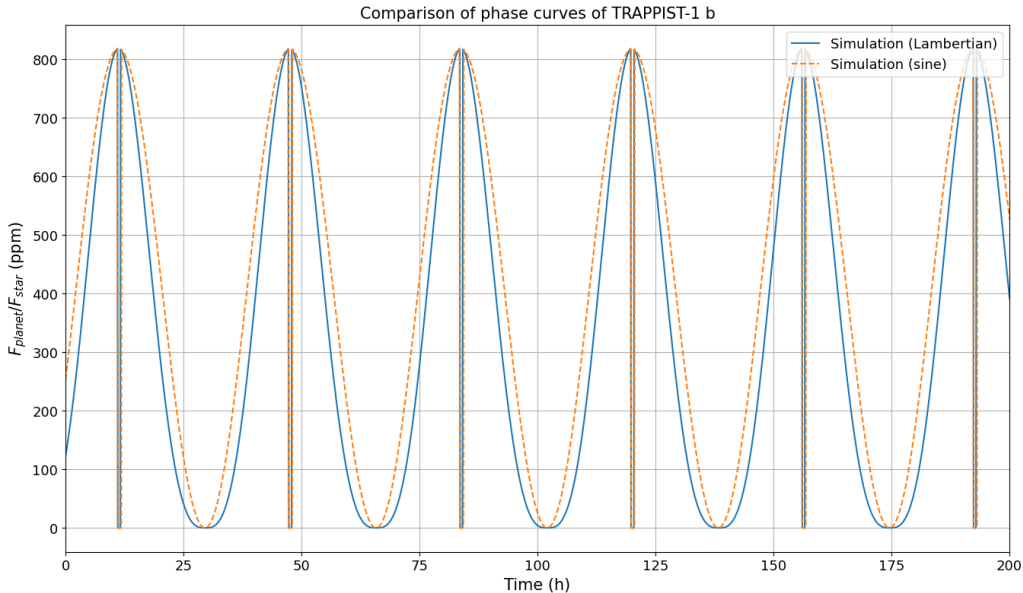


Figure 5: Comparison between the Lambertian model of the phase (Eq. 14) and the sine model (Eq. 15). Both of these simulations of the phase curve of TRAPPIST-1 b were made using bolometric fluxes (Eq. 12), supposing a bare-rock and a night side at 0 K.

The emitted flux from the planet day side that we would observe would then be  $F_{obs}(t) = F_{emitted} \cdot g(t)$ . However, in the case of a planet with full thermal redistribution, the night side would emit the same flux as the day side (see Eq. 8) so the phase curve would be flat. In my Exoplanet\_Phase\_Curve codes, that planetary flux is either expressed as a relative flux  $F_{planet}/F_{star}$  in ppm with respect to the stellar flux or as an absolute flux in mJy (see Section 2.2.2).

### 2.1.5 Transit timing variations

As TRAPPIST-1 is a system containing seven planets orbiting at a short distance from each other (see section 2.1.6), their motion cannot fully be considered as Keplerian as one planet and the star will be affected by the gravity of the other ones (see Figure 6). Consequently, the transits of this planet will not occur exactly at a frequency corresponding to the planet orbital period but a bit earlier or later than expected as shown in Figure 7.

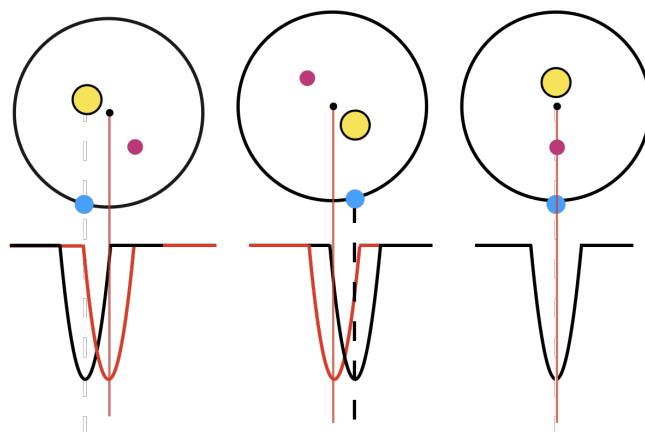


Figure 6: Illustration of the shift of the transits of one planet due to the gravitational effects of an other one. This second planet causes the barycenter of the system to not be aligned with the star and the transiting planet leading the transits to be shifted in time outside of the times when the three objects are simultaneously aligned in the observer's line of sight. (Figure provided by Elsa Ducrot)

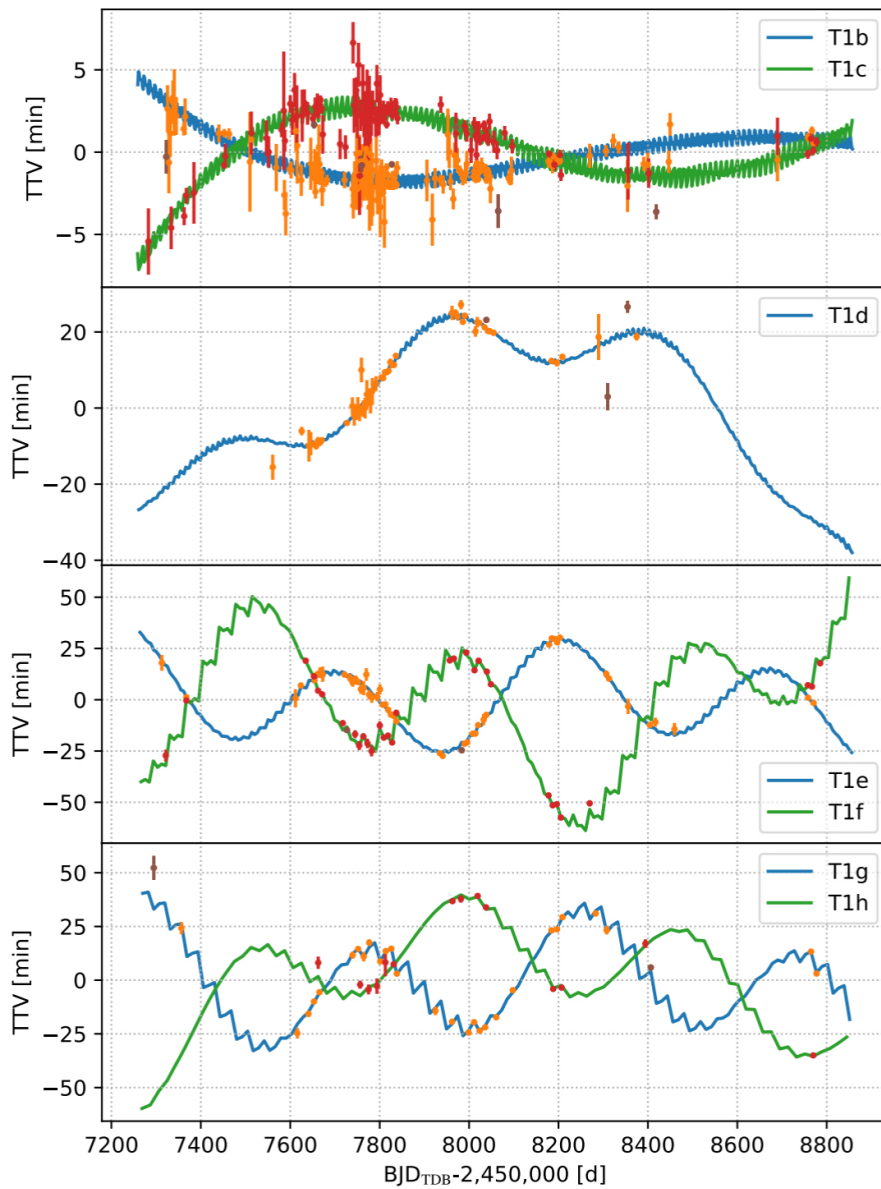


Figure 7: Transit-time model (blue and green lines) and TTV measurements (orange and red error bars) of the seven TRAPPIST-1 planets.  $> 3\sigma$  outliers are represented with the brown error bars. (Figure from [Agol et al. \(2021\)](#))

These deviations are called transit timing variations or TTVs. I will not enter into the details of how they are predicted, as it is out of the scope of my internship, but this is a phenomenon that must be taken into account to compare phase curve simulations with JWST observations ([Agol et al. 2021](#)) as otherwise the transits used as reference might not be at the expected times.

### 2.1.6 Overview of the TRAPPIST-1 system

The TRAPPIST-1 star is an M8-type star at 12.42 parsecs (or about 40 light-years) from the Solar System in the Aquarius constellation. The values of its physical properties that I used in `Exoplanets_Phase_Curve` are in Table 1:

Physical property	Value	Reference
Effective temperature (K)	$2566 \pm 26$	<a href="#">Agol et al. 2021</a>
Radius ( $R_{\odot}$ )	$0.1192 \pm 0.0013$	<a href="#">Agol et al. 2021</a>
Mass ( $M_{\odot}$ )	$0.0898 \pm 0.0023$	<a href="#">Ducrot et al. 2020</a>
Luminosity ( $L_{\odot}$ )	$10^{-3.26 \pm 0.01}$	<a href="#">Ducrot et al. 2020</a>

Table 1: Physical properties of star TRAPPIST-1 from the NASA Exoplanet Archive website with  $R_{\odot} = 6.96 \cdot 10^8$  m,  $M_{\odot} = 2 \cdot 10^{30}$  kg and  $L_{\odot} = 3.83 \cdot 10^{26}$  W.

The seven known planets orbiting star TRAPPIST-1, discovered by [Gillon et al. \(2017\)](#), have semi-major axes between about 0.01 and 0.06 astronomical units with orbital periods extending from about 1.5 to 18 days [\(Ducrot et al. 2020\)](#). This makes this system far more compact than our Solar System with all the planets being much closer to their star than Mercury to the Sun. However, since TRAPPIST-1 is a much cooler star than the Sun, its habitable zone is also much closer, so that planets e to g are within it [\(Turbet et al. 2018\)](#), with TRAPPIST-1 e being considered to have the most potential to harbor liquid water on its surface [\(Fauchez et al. 2020\)](#).

Moreover, this compactness is the cause of strong gravitational interactions between planets leading to the TTVs explained in section 2.1.5. It is also the cause of a Laplace orbital resonance chain which strongly amplifies the TTVs, making them easier to measure [\(Luger et al. 2017\)](#). This also permits to have more precision on the planetary masses constraints. Furthermore, the short distance between the planets and their star is also source of tidal locking, i.e a synchronization between their rotation and their revolution around the star [\(Gillon et al. 2017\)](#). The exact physical properties of the TRAPPIST-1 planets I used for my codes during my internship are shown in Table 2:

Planet	$a (R_*)$	$P$ (days)	$i$ (°)	$\omega$ (°)	$e$	$R (R_{\oplus})$
b	20.13 <sup>a</sup>	1.51088432 <sup>a</sup>	89.28 <sup>a</sup>	336.86 <sup>b</sup>	0.00622 <sup>b</sup>	1.116 <sup>c</sup>
c	27.57 <sup>a</sup>	2.42179346 <sup>a</sup>	89.47 <sup>a</sup>	282.45 <sup>b</sup>	0.00654 <sup>b</sup>	1.097 <sup>c</sup>
d	38.85 <sup>a</sup>	4.04978035 <sup>a</sup>	89.65 <sup>a</sup>	-8.73 <sup>b</sup>	0.00837 <sup>b</sup>	0.788 <sup>c</sup>
e	51.0 <sup>a</sup>	6.09956479 <sup>a</sup>	89.663 <sup>a</sup>	108.37 <sup>b</sup>	0.000510 <sup>b</sup>	0.920 <sup>c</sup>
f	67.10 <sup>a</sup>	9.20659399 <sup>a</sup>	89.666 <sup>a</sup>	368.81 <sup>b</sup>	0.01007 <sup>b</sup>	1.045 <sup>c</sup>
g	81.7 <sup>a</sup>	12.35355570 <sup>a</sup>	89.698 <sup>a</sup>	191.34 <sup>b</sup>	0.00208 <sup>b</sup>	1.129 <sup>c</sup>
h	107.9 <sup>a</sup>	18.76727450 <sup>a</sup>	89.763 <sup>a</sup>	338.92 <sup>b</sup>	0.00567 <sup>b</sup>	0.755 <sup>c</sup>

Table 2: Some physical properties of the TRAPPIST-1 planets from the NASA Exoplanet Archive website. The stellar radius of TRAPPIST-1  $R_*$  corresponds to the one in Table 1 and the Earth radius is  $R_{\oplus} = 6378$  km. Since I did not use them in my codes and for better readability, the uncertainties are not shown here. (References: <sup>a</sup>: [Ducrot et al. \(2020\)](#), <sup>b</sup>: [Grimm et al. \(2018\)](#), <sup>c</sup>: [Agol et al. \(2021\)](#))

## 2.2 Simulation of phase curves using Python

### 2.2.1 Working hypotheses

As we saw in section 2.1.4 many parameters have an influence on the phase curve of an exoplanet. However, in order to build our model, we can make several simplifying hypotheses.

First, we will ignore the limb-darkening of the star. We can make this hypothesis as this phenomenon will have little impact on the data we will work with. Indeed, we will use observations of an M-type star in the mid-infrared domain so limb darkening will be far less important than if we worked in the visible. Furthermore, our data comes from eclipses and limb darkening mainly impacts transits.

On another hand, even if considering the star as a black body is a good first approximation, it still differs from reality, so instead of using Planck's law (Eq. 7) to establish the star spectrum, we will use spectral grids from the SPHINX (Iyer et al. 2022) and PHOENIX (Allard et al. 2012) models in order to get a result closer to the JWST observations (see Figure 8).

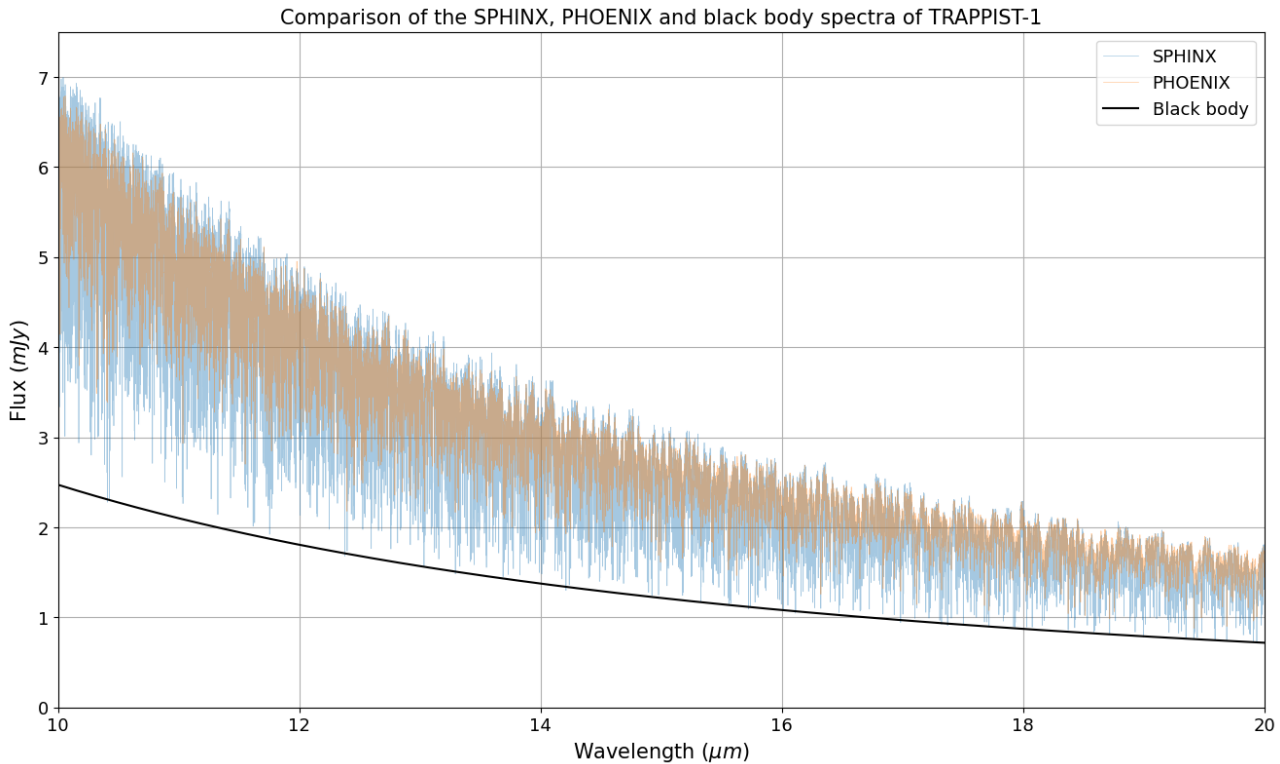


Figure 8: Comparison between the spectrum of a black body (in black) and the SPHINX (in blue) and PHOENIX (in orange) models at 2566 K over the wavelength range we are interested in.

The planets, on the other hand, can still be described as black bodies and we will consider that their Bond albedos are equal to 0. Furthermore, we will only consider the two extreme cases mentioned in Section 2.1.3: 1) a thermal redistribution between the day and night sides equal to zero, leading the temperature of the night side to be equal to 0 K, which would correspond to an airless planet, and 2) a full redistribution, leading the day and night side temperatures to be equal, which would correspond to the case of a planet with a thick atmosphere. In the case of an airless planet, I also considered that the temperature is homogeneous all over the day side, which is obviously not the case in reality, as the received flux at the surface would decrease as we get further from the sub-stellar point.

A planet as a bare rock will thus have a phase curve following Eq. 15 while the one of a planet with a thick atmosphere will be completely flat (except during eclipses) with a flux corresponding to the temperature computed using Eq. 8.

Furthermore, we can also make some assumptions about the orbital parameters of each planet. As shown in Table 2, the TRAPPIST-1 planets have very low eccentricities, so we can assume that they have circular orbits. Similarly, we can also consider that they have an inclination of 90°. However, as I wanted to do a general code to plot exoplanet phase curves that could be used for other planetary systems, I wrote the first code of Exoplanets\_Phase\_Curve with bolometric fluxes for elliptical and inclined orbits to be sure that this part of the code was working. I only assumed circular and non-inclined orbits afterwards, when I started working with the “real” stellar spectrum and the TTVs.

Finally, we will consider that during the eclipse the planetary flux is instantly put to zero during the total duration so we will only use Eq. 5.

### 2.2.2 Code overview

In this section, I will give a global overview of my strategy to simulate the phase curves of the TRAPPIST-1 planets in Python. However, I tried to write my codes in a way that they could easily be reused for other planetary systems without the simpler hypotheses on the orbits that I evoked in the previous section. I also made my codes available on GitHub at the following address so that they can be looked at, reused or even improved by others in the future: [https://github.com/LJ-Cartigny/Exoplanets\\_Phase\\_Curves](https://github.com/LJ-Cartigny/Exoplanets_Phase_Curves). More technical information about my codes can be found in Appendix B.

First, I needed a way to compute the true anomaly (Eq. 2) of each planet in order to determine their respective positions at a given time. For this, I solved the Kepler equation (Eq. 3) using the `optimize.fsolve` function of the Scipy library (Gommers et al. 2025). Then I used the computed true anomaly to compute the Lambertian phase (Eq. 13 and 14). I also implemented the sine model of the phase curve (Eq. 15) which is the one that I used for my simulations in the end.

To compute the flux ratio  $F_{\text{planet}}/F_{\text{star}}$  between one planet and the star, I first used the bolometric fluxes (Eq. 12) as a first approach but then moved to the fluxes closer to reality by only integrating on the MIRI filters bandpasses (see Section 2.3.1) and by replacing the black body spectrum  $B_\lambda$  of Eq. 9 by the SPHINX or PHOENIX models as said in Section 2.2.1.

This ratio can be used to compute the absolute flux of the planet in mJy. Indeed, we can first estimate the absolute flux of the star in mJy by integrating the SPHINX or PHOENIX spectrum over the filter's bandpass. As this flux is supposed to be constant, we can multiply it by the variations of the flux ratio to get the absolute planetary flux. In order to set the minima of the phase curve at the flux of the star alone, I rather computed and plotted the sum  $(F_{\text{star}} + F_{\text{planet}})_{\text{mJy}}(t) = (F_{\text{planet}}/F_{\text{star}} \cdot g(t) + 1) \cdot F_{\text{star,mJy}}$ , with  $g(t)$  the phase of the planet at time  $t$  (see Eq. 15).

I also had to place the eclipses at the maxima of the phase curve. To do so, I used Eq. 5 to compute the full duration of an eclipse. I then used this duration to determine the phase at which the eclipse begins and the one at which it ends. By checking if the current phase of the planet is in this interval or not, I created a Boolean that sets the flux ratio  $F_{\text{planet}}/F_{\text{star}}$  to zero when the planet is eclipsed. As I was first working with relative fluxes in the case of bare rocks, I did not have to implement the transits, as they would occur at the minima of the phase curve when the flux ratio would be null. It would then have been necessary to implement them later for simulations with an atmosphere, as the flux from the night side would then not be equal to zero, and when I studied the case of an absolute flux, since the total flux  $F_{\text{planet}} + F_{\text{star}}$  would decrease during a transit because the planet blocking part of the stellar flux (see Section 2.1.2). However, the data that I had to analyze were only coming from eclipses (see Section 2.3.1), so I decided not to show the transits on my phase curves plots for better clarity. They could yet be easily implemented using a similar way as for the eclipses.

In practice, my code can simulate phase curves of several specified planets (and the sum of their respective signals) starting from a given time (expressed in  $\text{BJD}_{\text{TBD}} - 2450000$ ) for a given number of days with the planetary fluxes set to zero during the eclipses. It is possible to specify if the result (which can be saved in a .txt file) has to be expressed using relative fluxes in ppm or absolute fluxes in mJy, if the thermal redistribution must be set to 0 (for a case without atmosphere) or to 1 (for a case with a thick atmosphere) and which stellar spectrum model (SPHINX or PHOENIX) and which MIRI filter to use.

It only requires several parameters: the mass, radius and a spectrum model of the star; the planet's semi-major axis, orbital period, inclination, eccentricity, argument of pericenter and radius; the bandpass of the spectrum. If we want to use absolute fluxes in mJy, it also requires the distance between the system and Earth. Finally, it needs the time of at least one known transit of each planet (even if more is recommended due to the TTVs).

To know the transit that serves as a reference, my code locates the nearest transit from the  $t_0$  of the simulation in a file provided by my supervisors containing transit predictions from [Agol et al. \(2021\)](#) which take the TTVs into account. If they had not been taken into account, the predicted times of the eclipses and transits would be wrong as the shifts can reach up to 100 minutes after a year. Initially, I wanted to use these predictions to have an adaptive orbital period in my simulation that would be modified after each transit to take into account the TTVs. Unfortunately, I encountered too many problems trying to do this and I eventually rather used the Keplerian period to avoid losing too much time on this and in the end the transit predictions with TTVs ended up being only used for finding the nearest transit from the simulation beginning. As a result, the timings of the transits and eclipses in my simulations may be a little bit shifted with respect to the actual ones if the simulation spreads over a long period of time.

## 2.3 Analysis of JWST data

### 2.3.1 Dataset and instrument used

The data I used during my internship comes from the Mid-InfraRed Instrument (MIRI) ([Rieke et al. 2015](#)) of the JWST. It was produced during photometric observation programs between October 2022 and December 2024 using MIRI F1280W and F1500W filters which have effective wavelengths around  $12.8\ \mu\text{m}$  and  $15\ \mu\text{m}$  respectively. Their complete bandpasses are shown in Figure 9:

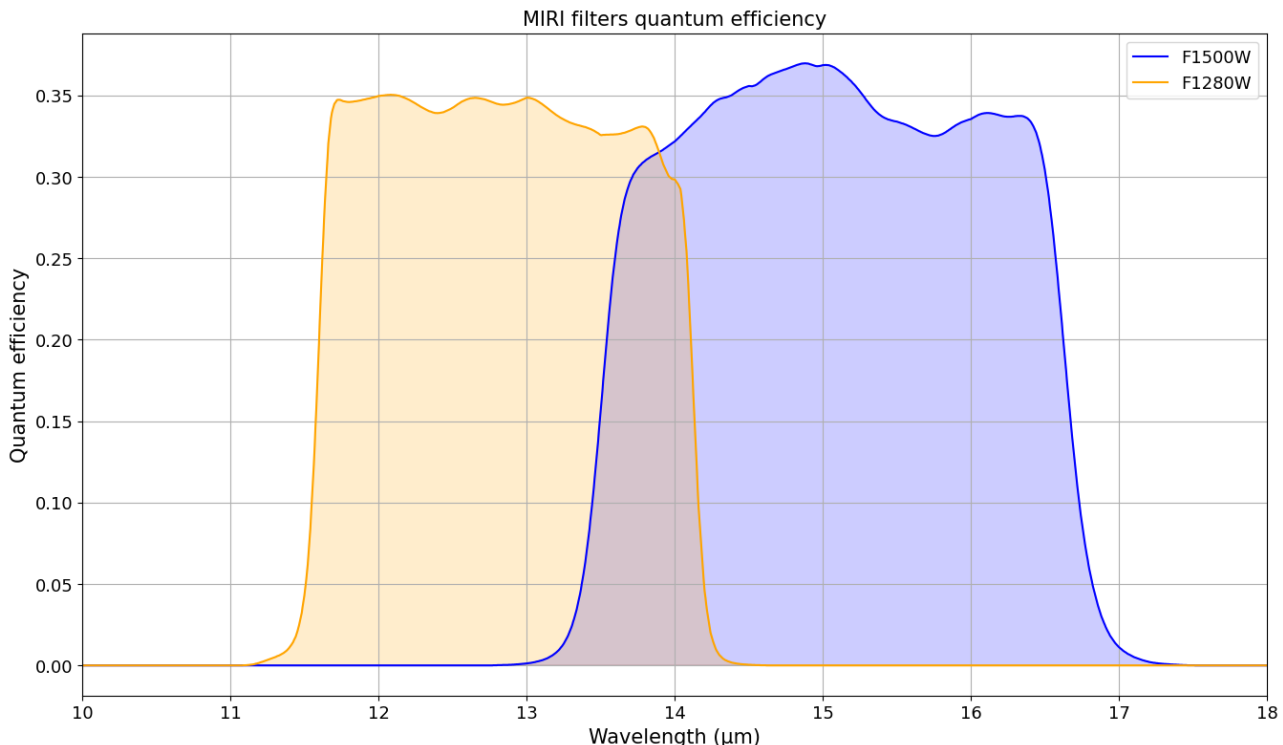


Figure 9: The bandpasses of MIRI F1280W and F1500W filters

To take into account these bandpasses, we need to modify Eq. 9:

$$\frac{F_{planet}}{F_{star}} = \left( \frac{R_{planet}}{R_{star}} \right)^2 \frac{\int_{\lambda_1}^{\lambda_2} E(\lambda) \cdot B_\lambda(T_{planet}) d\lambda}{\int_{\lambda_1}^{\lambda_2} E(\lambda) \cdot S(\lambda) d\lambda} \quad (16)$$

with  $E(\lambda)$  the normalized quantum efficiency of the filter at wavelength  $\lambda$  and  $S(\lambda)$  the stellar spectrum model used (SPHINX or PHOENIX).

An overview of each observation program from which I used its data is shown in Table 3:

Program ID	Target(s)	MIRI filter	Reference
GTO 1177	5 eclipses of TRAPPIST-1 b	F1500W	<a href="#">Greene et al. (2023)</a>
GTO 1279	5 eclipses of TRAPPIST-1 b	F1280W	<a href="#">Ducrot et al. (2024b)</a>
GO 2304	4 eclipses of TRAPPIST-1 c	F1500W	<a href="#">Zieba et al. (2023)</a>
GO 3077	Phase curves of TRAPPIST-1 b and c	F1500W	<a href="#">Gillon (2024)</a>
GO 5191	4 simultaneous eclipses of TRAPPIST-1 b and c	F1280W	<a href="#">Ducrot et al. (2024a)</a>

Table 3: Information about all the JWST MIRI imaging photometric observations programs of TRAPPIST-1 b and c

Complementary information about these observations can be found in Appendix C.

### 2.3.2 The Eureka! pipeline

In addition to stellar flux values directly given by my supervisors that were measured during the eclipses observed by the programs in Table 3, I also analyzed some of the JWST data to derive the light curve from the photometric images by myself. For this, I used the Eureka! pipeline ([Bell et al. 2022](#)) which was mainly designed to reduce and analyze JWST data for exoplanet observations. It is divided into six different parts or 'Stages' that are summarized here in the case of a photometric study:

- Stages 1 & 2: calibrate the raw JWST data;
- Stage 3: uses the calibrated data to perform aperture photometry and extract a light curve;
- Stage 4: uses the Stage 3 output and removes the outliers and takes effects such as the drift, jitter or limb-darkening into account to improve the light curve;
- Stage 5: fits the light curve in output of Stage 4 with noise and astrophysical models using several optimization and sampling algorithms;
- Stage 6: generates additional figures and tables from the results of the Stage 5 fit.

During my internship, I downloaded JWST data on the Mikulski Archive for Space Telescopes (MAST) that has already been calibrated so I did not have to run Stages 1 and 2 of the Eureka pipeline. I also did not need the additional figures from Stage 6 so I only ran Stages 3, 4 and 5 that I will briefly present here (more information about each step can be found in the Eureka! documentation).

Stage 3 performs aperture photometry. This technique consists of measuring the flux coming from a disk containing the target while estimating the background/sky contribution by measuring the flux from a annulus-shaped area around it for each image (see Figure 10). I chose to use an aperture with a radius of 10 pixels for the target and an inner radius of 20 pixels with a width of 30 pixels for the sky.

During Stage 4, I considered that the effects of the drift/jitter of the JWST were negligible and, as explained in Section 2.2.1, limb-darkening was not taken into account in this study, as we do not study transits. So to improve the light curve I decided only to remove the outliers. I arbitrarily set the limit over which a point was considered as an outlier at  $6\sigma$  from the median, which is a conservative threshold.

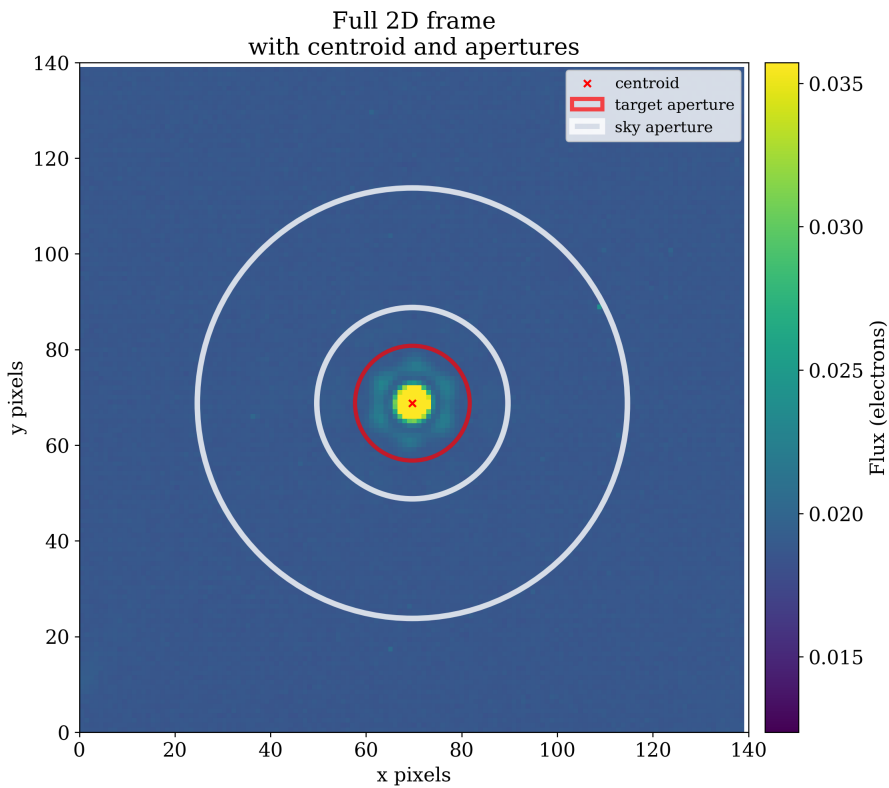


Figure 10: Aperture photometry used during Eureka! Stage 3 of the data analysis of the GO 3077 JWST observation program. The target flux is estimated from inside the red circle (which has a radius of 12 pixels) while the background contribution is estimated using the area between the two white circles (which have radii of 20 and 45 pixels).

Stage 5 allows to fit the data using routines such as the least-square method from SciPy ([Gommers et al. 2025](#)), nested sampling with dynesty ([Higson et al. 2019](#)) or the EMCEE sampler ([Foreman-Mackey et al. 2013](#)). As we cannot derive error bars from the least squared method (for this we need to get the posterior distributions), I had to choose between dynesty and EMCEE. In the end decided to use the latter because it seemed to be the most convenient for a first use of Eureka!.

### 2.3.3 Bayesian inference and MCMC

In this section, I will try to give a brief introduction to the Bayesian inference and the Markov chain Monte Carlo (MCMC) method that are used in the EMCEE code basing myself upon [Ducrot \(2021\)](#).

The goal of Bayesian inference is to estimate the probability distribution of a set of parameters in hypothesis from observed data using Bayes' theorem ([Bayes 1763](#)):

$$P(H|D) = \frac{P(H) \cdot P(D|H)}{P(D)} \quad (17)$$

where:

- $P(H)$ , called the prior probability, is the probability that the hypothesis  $H$  is observed (before we get the data);
- $P(H|D)$ , called the posterior probability, is the probability of our hypothesis  $H$  given the observed data  $D$  (after the observation). This function of  $H$  is what we want to know;
- $P(D|H)$ , called the likelihood, is the probability to observe the data  $D$  given the hypothesis  $H$ . It is a function of  $D$ ;

- $P(D)$  is called the marginal likelihood or model evidence. As it is not related at all to the hypothesis, this term can generally be ignored unless we want to compare several models.

The Bayes' theorem (Eq. 17) can thus be re-written as:

$$\text{posterior} = \frac{\text{prior} \cdot \text{likelihood}}{\text{marginal likelihood}} \quad (18)$$

If we consider two vectors  $\theta$  containing the model parameters and  $\mathbf{y}$  containing the observed data, the Bayes' theorem can be expressed as:

$$P(\theta|\mathbf{y}) = \frac{P(\theta) \cdot P(\mathbf{y}|\theta)}{P(\mathbf{y})} = \frac{P(\theta) \cdot P(\mathbf{y}|\theta)}{\int_{\theta} P(\theta)P(\mathbf{y})d\theta} \quad (19)$$

As the marginal likelihood can be ignored here, the expression of the joint posterior density can be written:

$$P(\theta|\mathbf{y}) = P(\theta) \cdot P(\mathbf{y}|\theta) \quad (20)$$

The posterior distribution for one parameter, also called marginal posterior distribution, can be expressed as the integral of this joint posterior density over all the other parameters:

$$P(\theta_i|\mathbf{y}) = \int P(\theta|\mathbf{y})d\theta_{j \neq i} \quad (21)$$

A good way to estimate the model parameters is by using Markov chain Monte Carlo (MCMC) sampling. This method is characterized by the randomness of the search, the Monte Carlo part, and the property that a proposed solution is based only on the previous step, the Markov part. Step by step, this process will build what is called a Markov chain. The longer the chain, the better the parameter distribution that we will compare with the data. The transition between one set of parameters to the next one is expressed as:

$$\theta_{n,j} = \theta_{i-1,j} + f\sigma_{\theta_j}G(0,1) \quad (22)$$

where  $j$  is the parameter,  $i$  the number of accepted steps and  $n$  the number of proposed steps. The term  $f\sigma_{\theta_j}G(0,1)$  is called the step size and corresponds to the difference between the next step and the current one with  $f$  a scaling factor that ensures that a certain percentage of step is accepted,  $\sigma_{\theta_j}$  the standard deviation of each transition parameter  $\theta_j$  and  $G(0,1)$  a Gaussian random number of mean and standard deviation respectively equal to 0 and 1.

At each step, a model  $\mu$  is generated from the output set of parameters  $\theta_n$  that we can compare with our data  $\nu$ . The goodness of the fit is estimated using the  $\chi^2$  statistics:

$$\chi_n^2 = \sum_{k=1}^l \frac{(\nu_k - \mu_k)^2}{\sigma_{\nu_k}^2} \quad (23)$$

where  $l$  is the total number of data points. To express our merit function, we need to add Bayesian penalties for the parameters for which we have prior knowledge expressed as  $\theta_{0,j} \pm \sigma_{\theta_{0,j}}$ . Assuming prior distributions are Gaussian, the merit function  $Q$  is:

$$Q_n^2 = \chi_n^2 + \sum_j \frac{(\theta_{n,j} - \theta_{0,j})^2}{\sigma_{0,j}^2} \quad (24)$$

A way to decide whether we accept or reject our new state  $\theta_n$  depending on our current state  $\theta_{i-1}$  is by using the Metropolis-Hastings algorithm ([Hastings 1970](#)). This algorithm considers that a new state  $\theta_n$  is acceptable if the likelihood that it describes the data is higher than the one of the previous state  $\theta_{i-1}$ . Thus we compute the likelihood ratio:

$$r = e^{-0.5(Q_n^2 - Q_{i-1}^2)} \quad (25)$$

Depending on the value of  $r$ , the new state is accepted or not:

- if  $r > 1$  the new state is accepted: a new  $n$  is proposed and  $i$  is incremented so that  $Q_i^2$  becomes the new  $Q_{i-1}^2$  and  $\theta_i$  the new  $\theta_{i-1}$ .
- else we draw a number  $u$  that is uniformly distributed between 0 and 1:
  - if  $u < r$  the step is rejected as  $Q_i^2 = Q_{i-1}^2$  and  $\theta_i = \theta_{i-1}$ . Then a new  $n$  is proposed and  $i$  is incremented but without changing  $Q_{i-1}^2$  and  $\theta_{i-1}$ .
  - if  $u > r$  the step is accepted as  $Q_i^2 = Q_n^2$  and  $\theta_i = \theta_n$ . Then a new  $n$  is proposed and  $i$  is incremented so that  $Q_i^2$  becomes the new  $Q_{i-1}^2$  and  $\theta_i$  the new  $\theta_{i-1}$ .

We repeat this process until  $i$  reaches the total number of steps (usually between 10000 and 50000).

The EMCEE code ([Foreman-Mackey et al. 2013](#)) uses this Metropolis-Hastings algorithm to accept or reject a new step. One particularity of this code is that it uses several Markov chains (called here walkers) simultaneously scattered across the parameters space, each new point of one chain being determined using the points of the others. This results in this code being generally more robust and faster to converge than the traditional MCMC codes. Furthermore, EMCEE is widely used to fit transits, eclipses and phase curves of exoplanets so to me it seemed a good choice for Eureka! Stage 5.

## 3 Results

### 3.1 Simulation of fluxes and phase curves

#### 3.1.1 General check with the bolometric fluxes

As said in Section 2.2, I first used bolometric fluxes to easily check if my code simulating phase curves was working in the general case, i.e with inclined and elliptical orbits. As shown in Figure 11, I managed to simulate the phase curves of the seven planets of TRAPPIST-1 with the eclipses occurring at the right time, i.e at the maxima, and each planet having the right orbital period (see Table 2).

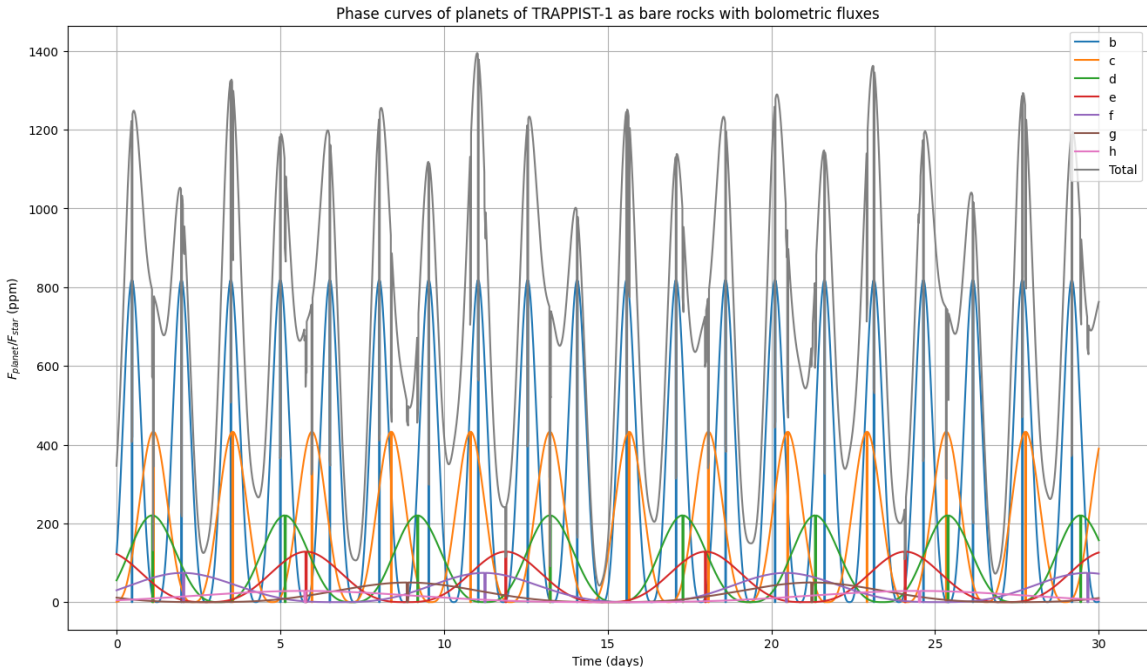


Figure 11: Simulation over 30 days of the phase curves of the seven planets of TRAPPIST-1 as bare rocks using relative bolometric fluxes with inclined and elliptical orbits. The total relative flux is also displayed. The drop at each maxima corresponds to the eclipses, during which the planetary flux is zero. The transits are not displayed as for bare rocks they would occur when the planets present their night sides, i.e when their fluxes would be zero.

### 3.1.2 Simulations of the JWST observations

Then I made a simulation using circular and non-inclined orbits over the whole time span covered by the JWST observations that interested me to estimate each planet contribution during these observations that are shown in color in Figures 12 and 13. This also permitted to check whether my simulations placed the JWST observations at the times corresponding to the targeted event (see Table 3). As we can see on the plots, the observations are correctly placed over the right events, which validates the simulations.

In Figure 13, I simulated the absolute fluxes of the outer planets only (without planets b and c), in order to estimate their combined contribution, in the F1500W MIRI filter and using the SPHINX model for the star. It is possible to see in this figure that if we want to have the highest difference in amplitude for the absolute fluxes coming from the outer planets it would be interesting to compare the visits 2 and 5 of the GTO 1177 program which uses the F1500W MIRI filter. It is also possible to take visits 3 and 5 of the GTO 1279 program if we want to rather use the F1280W filter (Figure 22 in Appendix A displays the same simulation but using the F1280W filter and the PHOENIX model).

The shared minimum of all the individual phase curves for each outer planet at around 2.55751 mJy corresponds to the flux of the star alone, integrated over the F1500W MIRI filter using the SPHINX model. We can also notice that the simulation shows an eclipse of TRAPPIST-1 e occurring, respectively, at the very beginning or at the very end of visits 3 and 4 of the GO 2304 program, which is surprising as this program was supposed to observe eclipses of TRAPPIST-1 c and nothing else (see Table 3). After a check with my supervisors, it occurred that in reality visit 3 started during the egress period of an eclipse of planet e and that an eclipse of this planet actually occurred during visit 4 but as they were too shallow to be detected (it would have required about 15 visits with the F1500W filter to significantly detect them, with a  $5\sigma$  precision for bare rocks). This validates even more the simulations I made.

Figure 14 presents the same phase curves but in relative fluxes and using this time the F1280W filter. It is possible to see that the total contribution of the outer planets of TRAPPIST-1 can reach up to 400 ppm of the stellar flux. Flux variations of several hundreds of ppm can be detected by the JWST, provided that the observation lasts during the whole variation, which would require an enormous amount of time (the GO 3077 phase curve alone required 60 hours of continuous observation). The space telescope could thus determine whether the five outer planets of TRAPPIST-1 are all bare rocks, provided that the observation occurs at a time when their total flux would drop from a maximum to a minimum (or the opposite).

## 3.2 Data from JWST observations

### 3.2.1 Analysis with Eureka!

I ran Eureka! Stages 3 to 5 on several visits of the GTO 1177 program, as they are the closest to the extrema of the total flux. However, despite having quite good fits the different parameters (see Figure 15), a strong ramp effect still remains at the beginning of the light curve obtained after Stage 5 as visible in Figure 16.

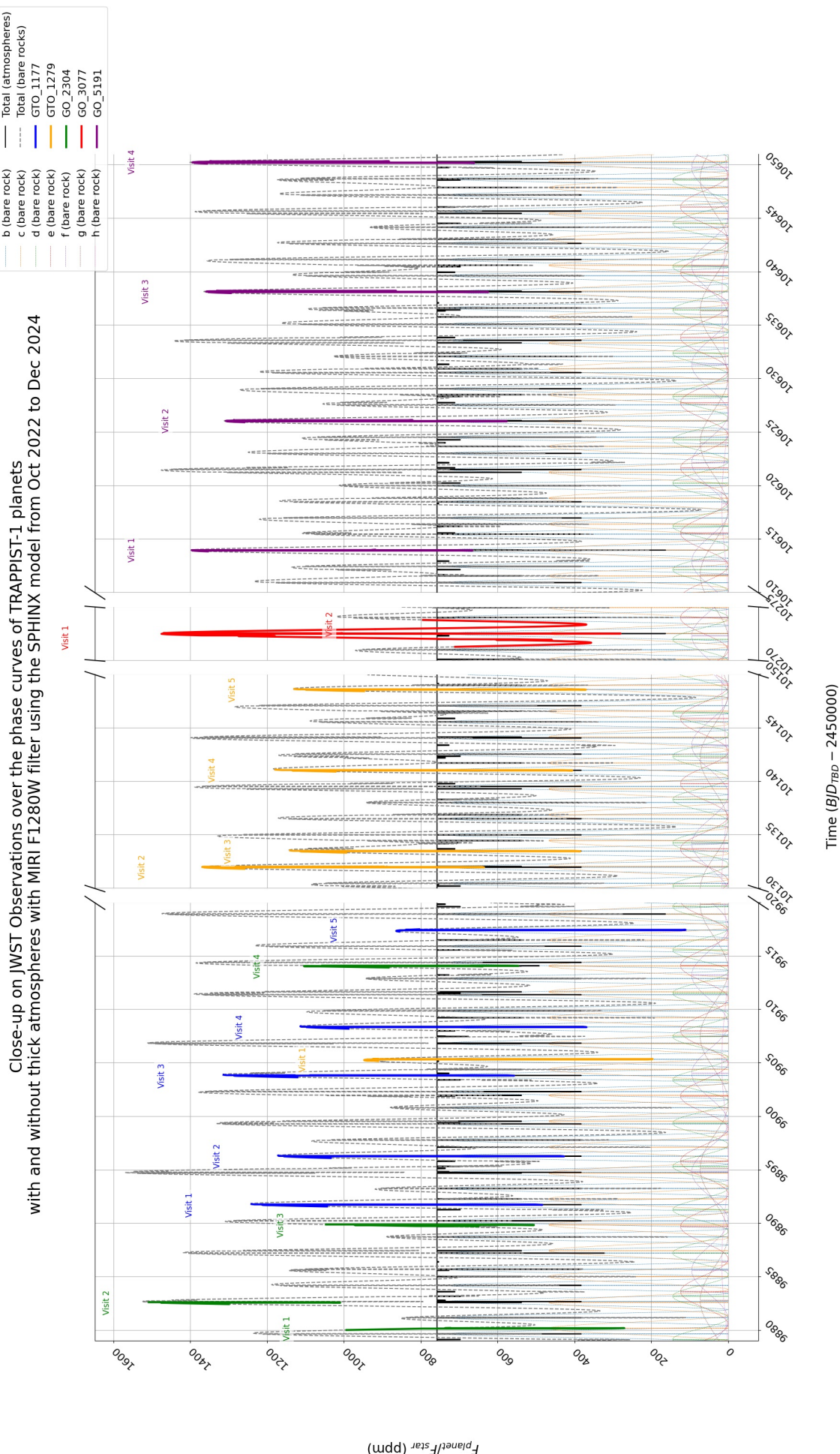


Figure 12: Simulation of the phase curves of the seven planets of TRAPPIST-1 in relative fluxes ( $F_p/F_s$ ) using the SPHINX model for the F1280W MIRI filter. The JWST observations are displayed in color over the total curve for the bare rock case. The flux of each planet as a bare rock is displayed to show its phase over time.

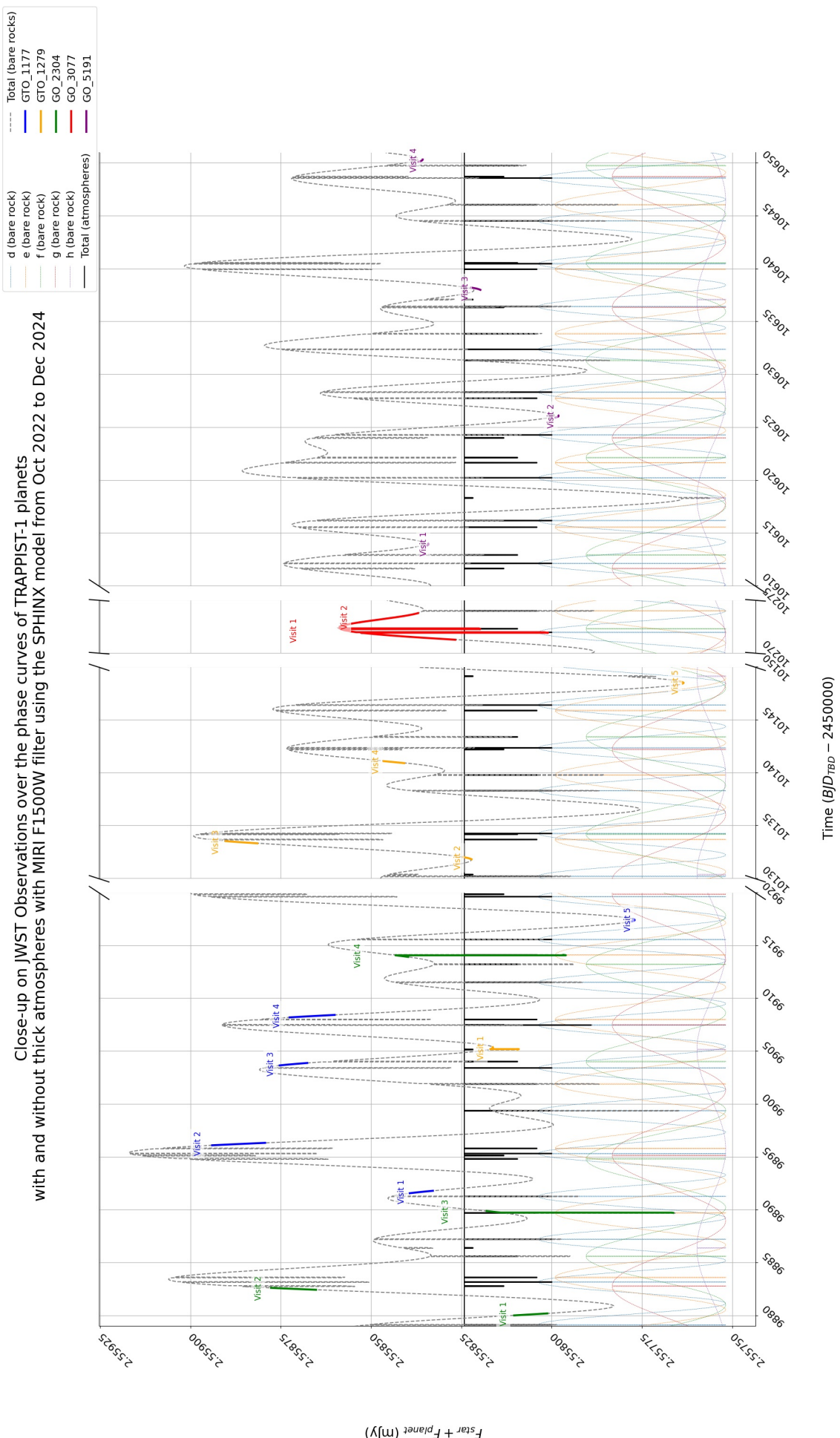


Figure 13: Simulation of the phase curves of the outer planets of TRAPPIST-1 in absolute fluxes using the SPHINX model for the F1500W MIRI filter. Transits are not displayed for better readability. The JWST observations are displayed in color over the total curve for the bare rock case. The flux of each outer planet as a bare rock is displayed to show its phase over time.

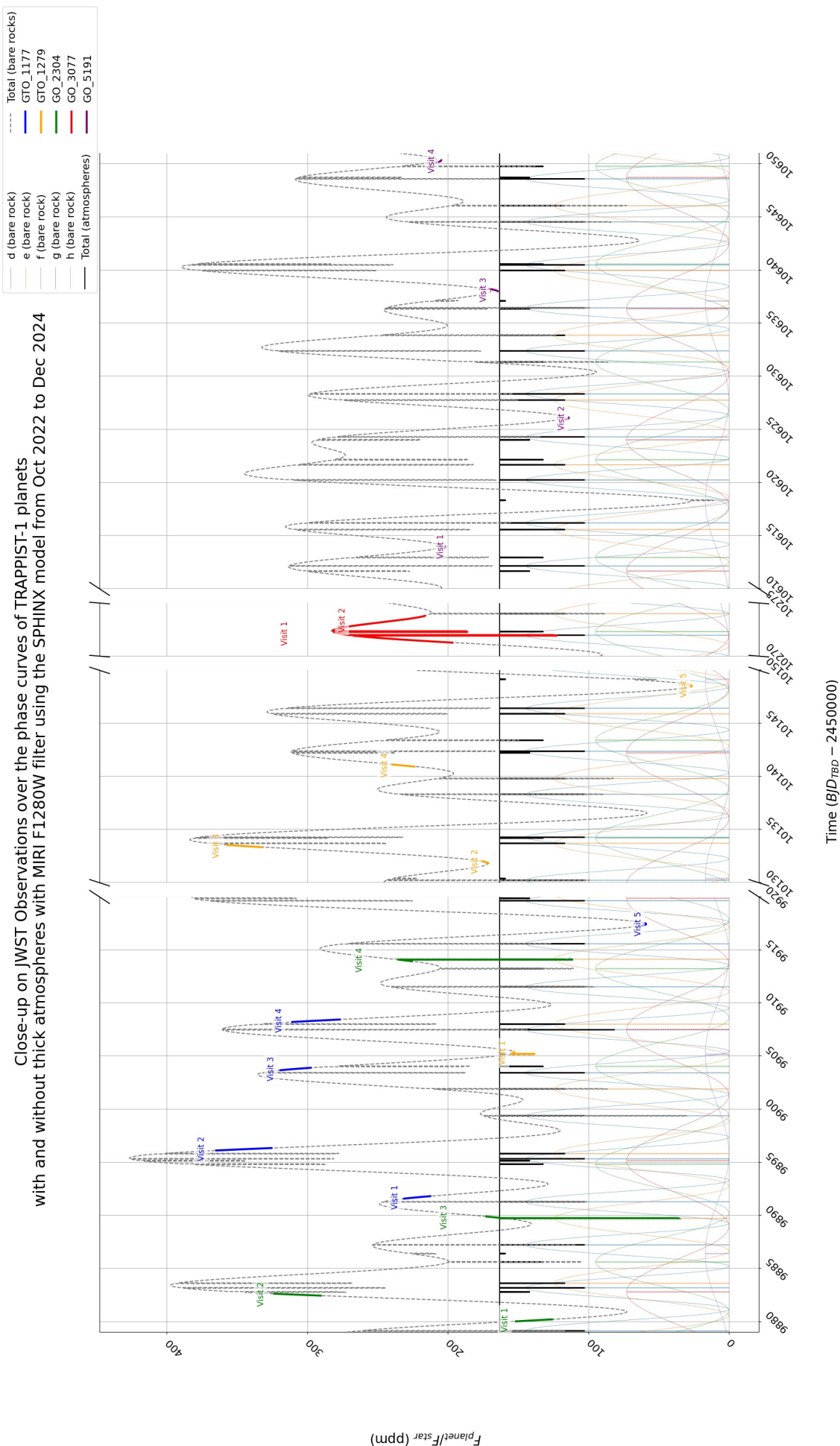


Figure 14: Simulation of the phase curves of the outer planets of TRAPPIST-1 in relative fluxes using the SPHINX model for the F1500W MIRI filter. The times of the JWST observations are displayed in color over the total curve for bare rocks case. The flux of each outer planet as a bare rock is displayed to show its phase over time.

### 3 Results

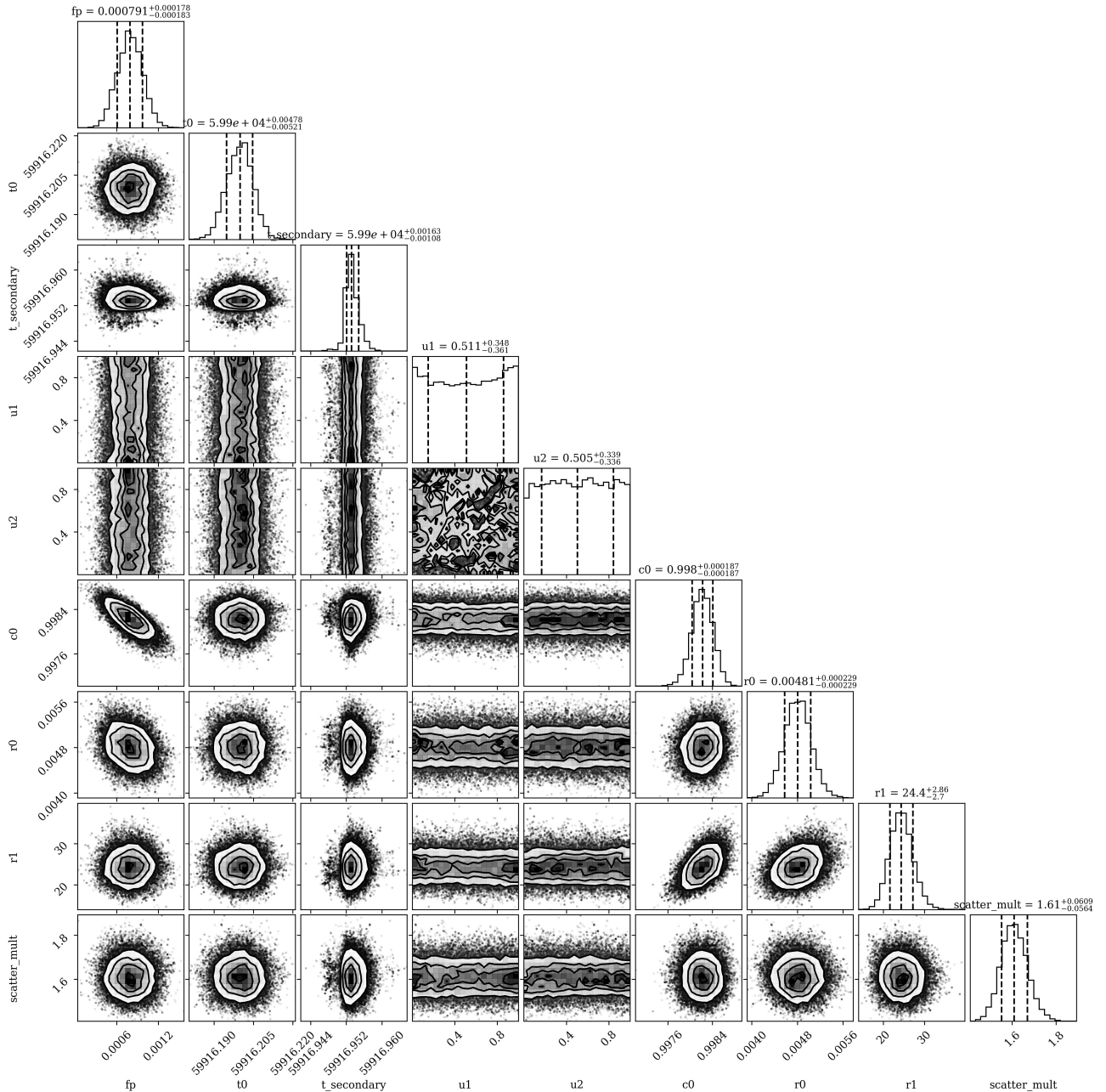


Figure 15: Fitted parameters after running Eureka! Stage 5 on data from visit 5 of the GTO 1177 program. They all converged towards a Gaussian distribution (or quite close) meaning that the fit is good.

This ramp effect is purely of instrumental origin and is very hard to model analytically, as it only depends on the history of the detector (previous target that was observed, orientation of the telescope, etc.) (Dyrek et al. 2024); (Bell et al. 2023). However, since it only affects the beginning of the observation, it should be far less important on longer observations such as the complete phase curves of TRAPPIST-1 b and c from the GO 3077 program. Such an instrumental systematic effect has been reported in several publications on JWST data, notably with MIRI LRS (Dyrek et al. 2024).

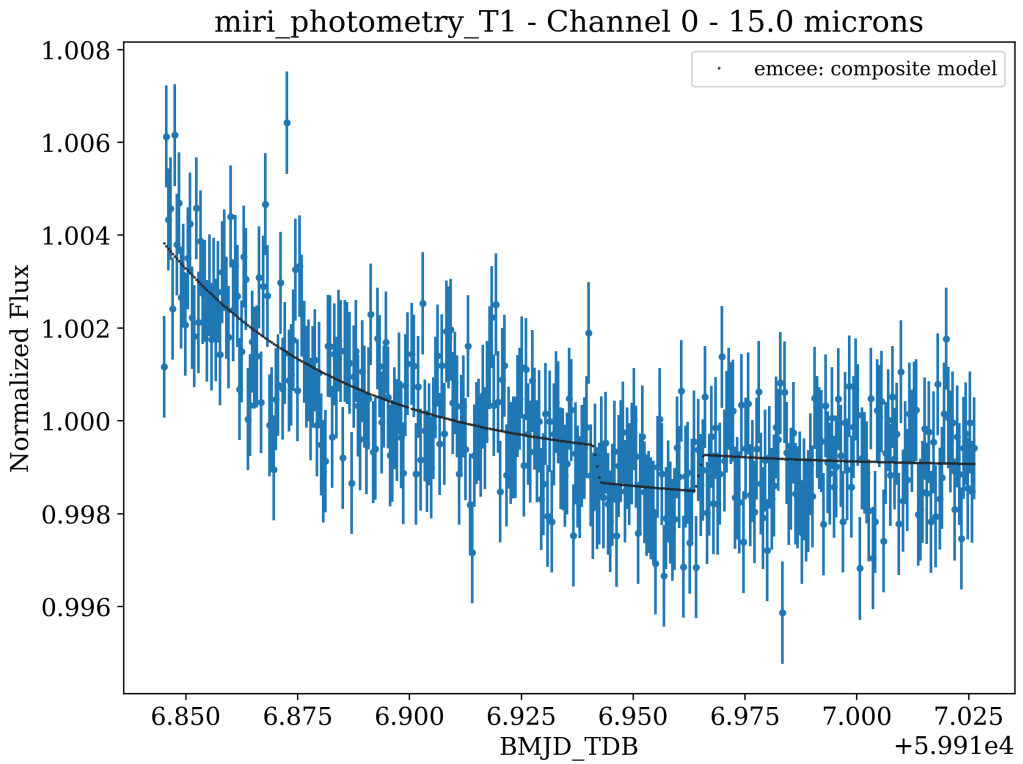


Figure 16: Light curve obtained after running the Stage 5 of Eureka! on data from visit 5 of the GTO 1177 program. Despite the eclipse of TRAPPIST-1 b being correctly detected, the remaining instrumental ramp effect is clearly visible at the beginning of the curve.

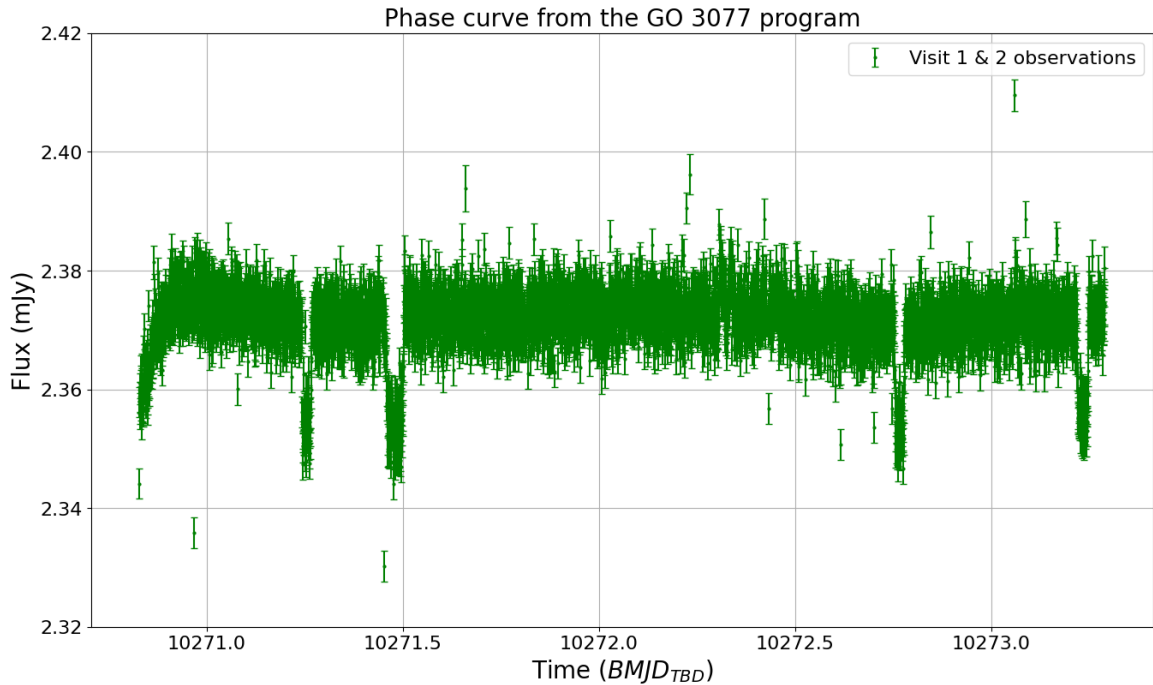


Figure 17: Phase curve of TRAPPIST-1 b and c obtained after running Stage 3 of Eureka! with the data from the GO 3077 program. The first and third transits correspond to planet b, the second one to g and the fourth to c.

Even if Stage 5 correctly modeled the ramp effect, I then only ran Stage 3 on the data from the GO 3077 program to be able to absolute fluxes in mJy as Stage 5 normalizes the fluxes which would then all be centered around 1. In Figure 17, it is possible to see that the ramp effect is very strong but,

as expected, it impacts a far less important part of the observation as here the observation is much longer. The transits of TRAPPIST-1 b, c and g are also clearly visible on the plot.

### 3.3 Comparisons

#### 3.3.1 Stellar fluxes comparisons

Previous studies have already shown that the SPHINX spectrum of TRAPPIST-1 differed from the observations by a factor of approximately 7% (Ducrot et al. 2024b); (Ih et al. 2023). I noticed the same shift before applying the right correction that permitted to place the simulated flux values inside the error bars of the observed values (see Figure 18). However, I also noticed that the PHOENIX spectrum had a similar shift of about 6.1% at  $12.8\ \mu\text{m}$  and 2.3% at  $15\ \mu\text{m}$ . This is consistent with a paper in preparation by Elsa Ducrot and Thomas Fauchez in which they explain that the 13% difference between the PHOENIX model and the observations from Greene et al. (2023) has been overestimated due to the use of an outdated version of the pysynphot Python library to generate the PHOENIX model. Consequently, I also applied a correction with PHOENIX in order to get the simulations closer to the observations.

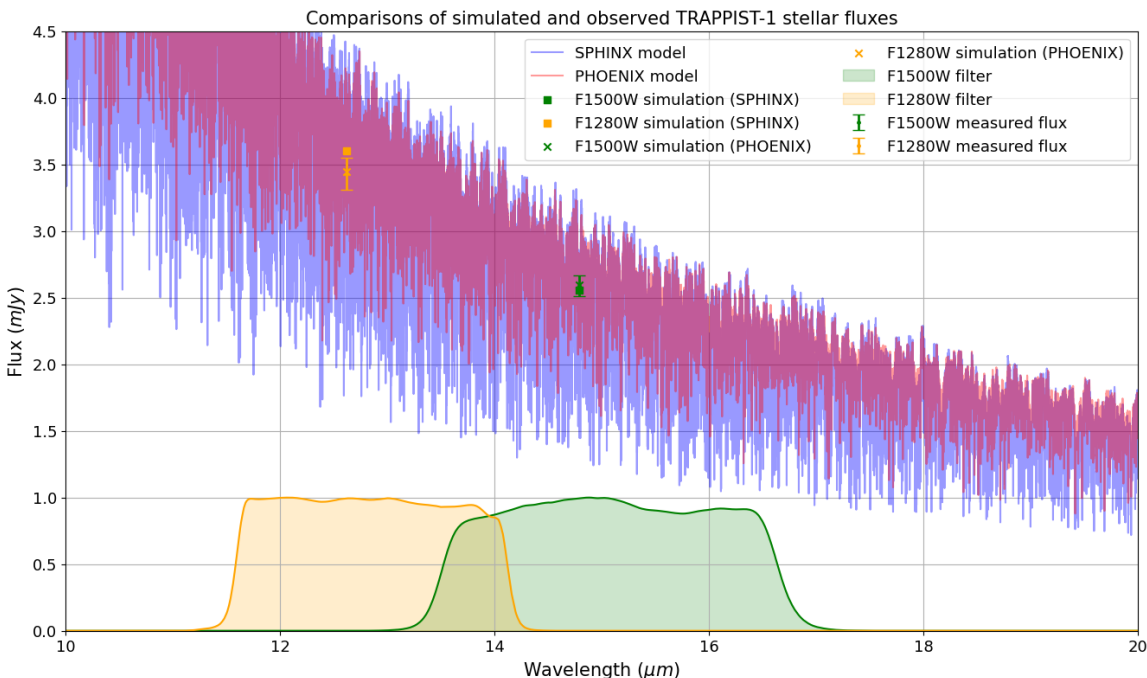


Figure 18: Comparison between the observed and simulated fluxes for the SPHINX and PHOENIX spectra. The values of the observed fluxes come from Ducrot et al. (2024b) for the F1280W filter and from Greene et al. (2023) for the F1500W filter.

#### 3.3.2 Placement of JWST observations over the simulated phase curves

To compare the fluxes measured by the JWST with my simulated phase curve, I started by placing a single data point for each visit corresponding to the sum of the planetary and stellar fluxes estimated during an eclipse. The exact flux values used for each visit can be found in Appendix C alongside other information about each JWST observation of TRAPPIST-1. I quickly noticed that the flux values of observations points were far lower than the simulated curve, such that the upper limits of the error bars did not even reach the level of the stellar flux alone, i.e the minima of the simulation. The origin of this difference is still unclear, as I could not determine whether it was coming from my code to integrate the simulated fluxes which would have overestimated the results or from the observations that would have underestimated the fluxes.

However, by looking at the comparison, it was clear that the error bars of the JWST observations (which correspond here to the most optimistic case with a 1% error (Gordon et al. 2024)) are far larger than the absolute flux variations due to the outer planets. To emphasize this difference, an offset was added to the data points from the observations in Figure 19. Additional figures showing data points from visits using the F1500W filter or using the SPHINX model for the simulation can be found in Appendix A. The reader can also regenerate these figures to be able to zoom inside them using the Exoplanets\_Phase\_Curves codes as explained in Appendix B. All these results show that unfortunately it is not possible to use previous JWST data to estimate the absolute flux contribution from the outer planets of TRAPPIST-1, as the uncertainties are far too important.

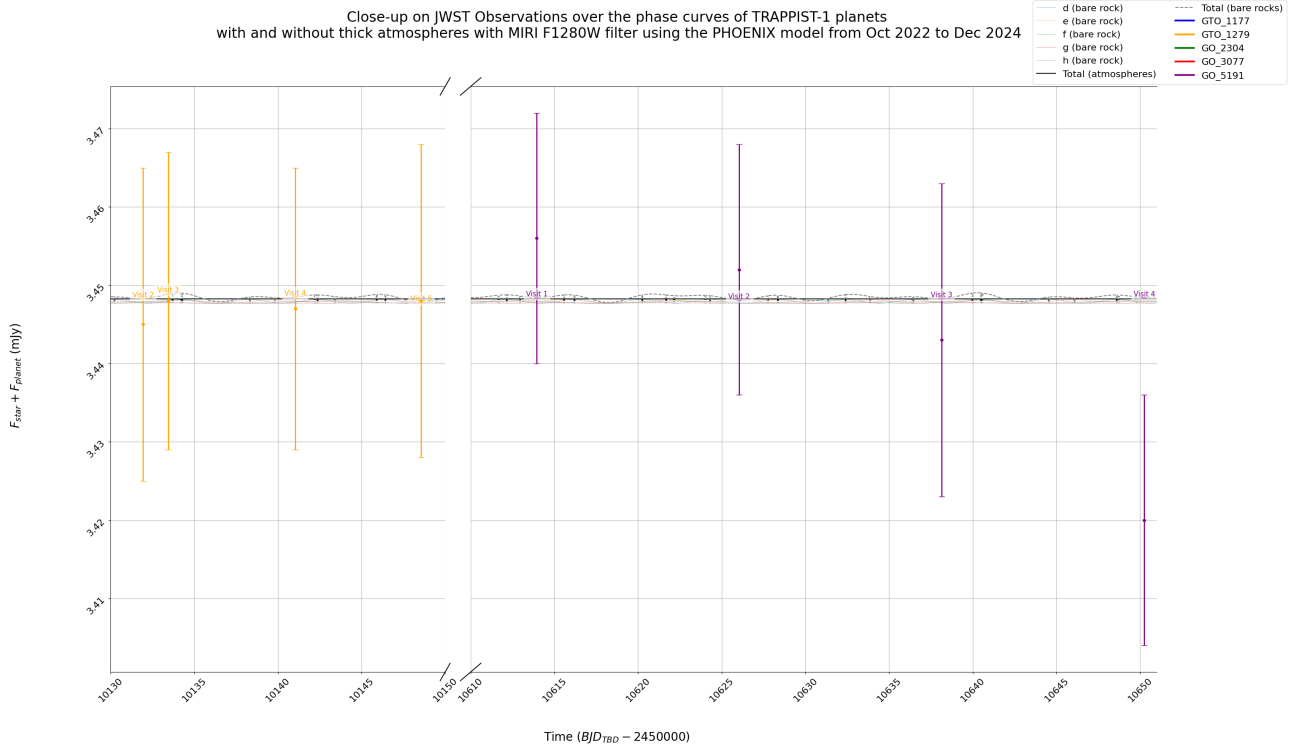


Figure 19: Comparison between the fluxes measured by the JWST and the simulated flux variations due to the outer planets of TRAPPIST-1 with the F1280W MIRI filter and the PHOENIX model. To place the data points at the same level than the phase curve, I added an offset of 0.02 mJy for GTO 1279 and 0.04 mJy for GO 5191. This figure only displays the visits that used the F1280W filter with results that were considered as usable.

Concerning the phase curve of the GO 3077 program treated with Eureka! Stage 3, I also obtained an offset with the simulations. I corrected it in Figure 20 in order to compare the shape of the curves although it might be possible to reduce this offset by using other parameters for Stage 3 treatment. Indeed, my first results had an even higher offset, but I managed to reduce it up to around 0.21 mJy by first modifying the photometric extraction method used by Eureka! (before that I had fluxes around 3.72 mJy which is far too high) and then the aperture radii, which modified the flux values by a few hundredths of mJy. The origin of this offset might be due to the fact that the precise absolute flux calibration with MIRI Imaging are still a topic of inquiry (Gordon et al. 2024).

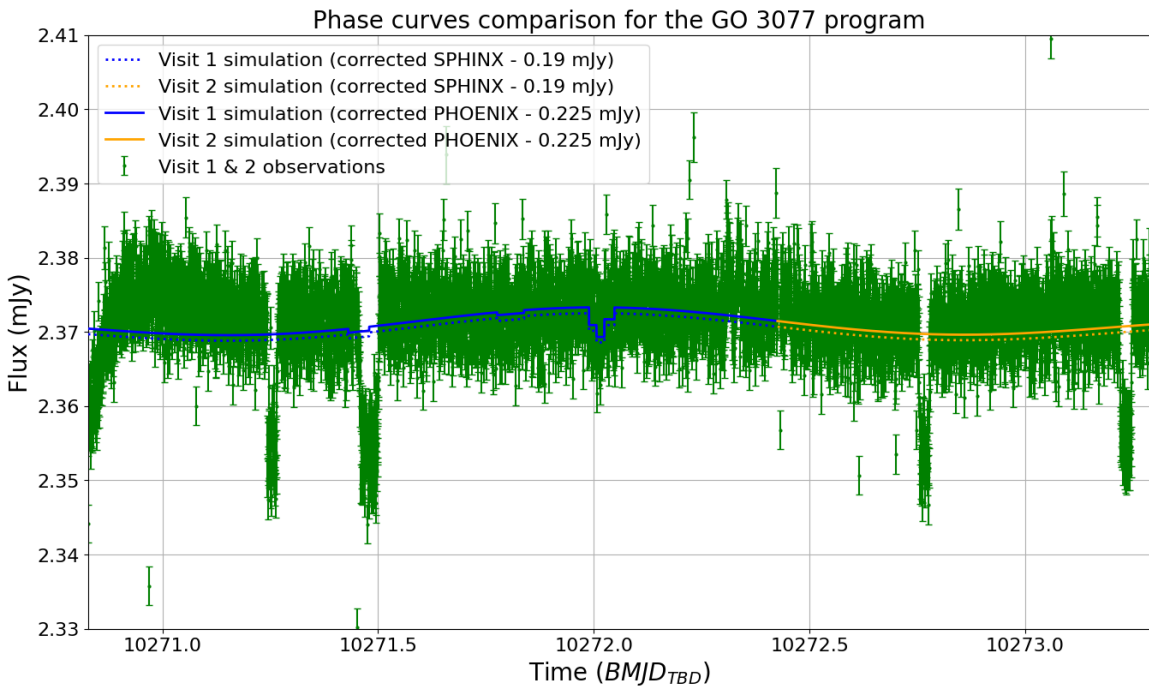


Figure 20: Comparison between the phase curve observed by the JWST during the GO 3077 program and the simulations of the total flux of star TRAPPIST-1 and its seven planets, using both the SPHINX and PHOENIX models. Offsets of  $-0.225$  mJy and  $-0.19$  mJy were respectively added to the simulations with the SPHINX and PHOENIX models in order to place these curves at the same level than the observations. As before, the transits are not displayed on the simulations

The simulated fluxes of Figure 20 contain this time the contribution of all seven planets of TRAPPIST-1 because, as the observation focused on the phase curves of planets b and c, the data contain the contribution of the two inner planets. Even without a fit, it is possible to notice that the simulations and the observation have the same variations over time.

## 4 Conclusion and perspectives

In the end, my study showed that detecting the absolute flux contribution of the outer planets of TRAPPIST-1 in previous JWST data was not possible due to large error bars. It would be interesting to try to estimate how much JWST observation time, i.e how many visits, it would require to reduce the error bars at a level low enough to distinguish our two extreme cases: all the outer planets as bare rocks or all with thick atmospheres. However, each of these visits would have to occur at a time where all the planets are in the same orbital configuration to observe the same fluxes every time, so it would also be necessary to estimate at what frequency it happens.

To reduce the error bars, another possibility might be to analyze the data of several visits of one program at once. We would then consider all these visits as a single observation with interruptions, similarly to the ground-based observations that are interrupted during the day. This would allow to work with relative fluxes and not absolute fluxes. It would require only one run of Eureka! but as the pipeline was not designed in that way we do not know if it will give coherent results.

Nevertheless, my results also show that the total contribution of the outer planets could be detected by the JWST in relative flux. This would require to make an long enough observation such that their total flux would vary of several hundreds of ppm. My Exoplanets\_Phase\_Curves code is suited to identify a moment with that kind of variations.

By developing `Exoplanets_Phase_Curves` I have shown that it is a very useful tool to simulate the phase curves of one or several exoplanets with our approximations. However, there are still several improvements that could be made. An important one would be to have a better implementation of the TTVs in order to have a better precision in the timings of the eclipses and transits by including a dynamical model that recalculate a new  $t_0$  and a new orbital period but it might be too consuming in processing time. Transits, and therefore limb darkening, could also be added for the simulation of phase curves in absolute flux. Another improvement that I did not complete was to consider, in the case of bare-rocks, the temperature of the day side of one planet as non-homogeneous and to make the temperature decrease as we move away from the sub-stellar point until it reaches zero at the terminator. These “eyeball” planets would be an approximation closer to reality. It would not be difficult to make small changes to my code so that it can easily be used for the study of other planetary systems, as I wrote my Python functions for the general case before making simplifications for TRAPPIST-1. Finally, I could add bridges with codes such as PLATON ([Zhang et al. 2024](#)) or the Planetary Spectrum Simulator (PSG) ([Villanueva et al. 2018](#)) to simulate different types of surfaces or atmospheres. I hope that these improvements will be made in the future, either by myself during a future internship or during my thesis, or by another intern or researcher who would find my code useful for their work. This is why I made my code fully available on GitHub so that anyone can access my code if they find it useful and/or want to make improvements.

To conclude, even if I did not manage during my internship to determine whether the outer planets of TRAPPIST-1 have atmospheres or not, I provided a code that can estimate the best moments to make new observations of this system with the JWST, as well as the expected flux variations, which might determine whether these Earth-sized planets have atmospheres.

## Acknowledgments

First, I would like to thank my two supervisors Alice Maurel and Elsa Ducrot for giving me the opportunity to do this internship which was exactly what I wanted to do. They were always available to help me and answer my questions when necessary and always made sure that my internship took place in the best conditions. Working with them gave me the confirmation that the study of Earth-sized exoplanets and of their atmospheres was the career I wanted to pursue. I hope to have the opportunity to work with them again in the future.

A big thank also to Estelle Chabrol with whom I shared an office during my time in Meudon. I enjoyed spending this time with her and wish her all the best for her thesis that will begin soon.

I also thank the exoplanets and planetology teams of the LIRA for their welcome and good times spent at lunch, as well as for all the very interesting seminars they organized during my time in Meudon.

I would also like to thank Martin Turbet (LMD) and Thomas J. Fauchez (NASA Goddard Space Flight Center) who helped me to find this internship and who then showed a lot of interest in my work.

I also thank the administrative teams of the IAP and Paris' Observatory for their help during the administrative work at the beginning of my internship.

Finally, I would like to thank my friends from the M1 SUTS for their support and their interest during my whole internship as well as the heads of the M1, Caroline Barban and Cédric Leyrat, who also always ensured that our internships took place in the best conditions.

## References

- Agol, Eric (Feb. 2007). "Rounding up the Wanderers: Optimizing Coronagraphic Searches for Extra-solar Planets". In: *Monthly Notices of the Royal Astronomical Society* 374, pp. 1271–1289. ISSN: 0035-8711. DOI: 10.1111/j.1365-2966.2006.11232.x. (Visited on 04/25/2025).
- Agol, Eric et al. (Feb. 2021). "Refining the Transit-timing and Photometric Analysis of TRAPPIST-1: Masses, Radii, Densities, Dynamics, and Ephemerides". In: *The Planetary Science Journal* 2, p. 1. ISSN: 2632-3338. DOI: 10.3847/PSJ/abd022. (Visited on 01/13/2025).
- Allard, F. et al. (June 2012). "Models of Very-Low-Mass Stars, Brown Dwarfs and Exoplanets". In: *Philosophical Transactions of the Royal Society A: Mathematical, Physical and Engineering Sciences* 370.1968, pp. 2765–2777. DOI: 10.1098/rsta.2011.0269. (Visited on 05/28/2025).
- Bayes, Thomas (Jan. 1763). "LII. An Essay towards Solving a Problem in the Doctrine of Chances. By the Late Rev. Mr. Bayes, F. R. S. Communicated by Mr. Price, in a Letter to John Canton, A. M. F. R. S". In: *Philosophical Transactions of the Royal Society of London* 53, pp. 370–418. DOI: 10.1098/rstl.1763.0053. (Visited on 04/23/2025).
- Bell, Taylor J. et al. (Nov. 2022). "Eureka!: An End-to-End Pipeline for JWST Time-Series Observations". In: *Journal of Open Source Software* 7.79, p. 4503. ISSN: 2475-9066. DOI: 10.21105/joss.04503. arXiv: 2207.03585 [astro-ph]. (Visited on 01/20/2025).
- Bell, Taylor J. et al. (Jan. 2023). *A First Look at the JWST MIRI/LRS Phase Curve of WASP-43b*. DOI: 10.48550/arXiv.2301.06350. arXiv: 2301.06350 [astro-ph]. (Visited on 06/16/2025).
- Cowan, Nicolas B. and Eric Agol (Dec. 2010). "A Model for Thermal Phase Variations of Circular and Eccentric Exoplanets". In: *The Astrophysical Journal* 726.2, p. 82. ISSN: 0004-637X. DOI: 10.1088/0004-637X/726/2/82. (Visited on 05/13/2025).
- Ducrot, Elsa (Aug. 2021). "Search for Habitable Planets Eclipsing Ultra-Cool Stars". PhD thesis. (Visited on 03/10/2025).
- Ducrot, Elsa et al. (Aug. 2020). "TRAPPIST-1: Global Results of the Spitzer Exploration Science Program Red Worlds". In: *Astronomy and Astrophysics* 640, A112. ISSN: 0004-6361. DOI: 10.1051/0004-6361/201937392. (Visited on 02/05/2025).
- Ducrot, Elsa et al. (Feb. 2024a). "Bare Rocks Are Not Supposed to Do That". In: *JWST Proposal. Cycle 3*, p. 5191. (Visited on 01/13/2025).
- Ducrot, Elsa et al. (Dec. 2024b). "Combined Analysis of the 12.8 and 15 μm JWST/MIRI Eclipse Observations of TRAPPIST-1 b". In: *Nature Astronomy*. ISSN: 2397-3366. DOI: 10.1038/s41550-024-02428-z. (Visited on 01/20/2025).
- Dyrek, A. et al. (Mar. 2024). "Transiting Exoplanets with the Mid-InfraRed Instrument on Board JWST: From Simulations to Observations". In: *Astronomy & Astrophysics* 683, A212. ISSN: 0004-6361, 1432-0746. DOI: 10.1051/0004-6361/202347127. (Visited on 06/16/2025).
- Fauchez, Thomas J. et al. (Feb. 2020). "TRAPPIST-1 Habitable Atmosphere Intercomparison (THAI): Motivations and Protocol Version 1.0". In: *Geoscientific Model Development* 13, pp. 707–716. ISSN: 1991-9603. DOI: 10.5194/gmd-13-707-2020. (Visited on 01/22/2025).
- Foreman-Mackey, Daniel et al. (Mar. 2013). "Emcee: The MCMC Hammer". In: *Publications of the Astronomical Society of the Pacific* 125.925, pp. 306–312. ISSN: 00046280, 15383873. DOI: 10.1086/670067. arXiv: 1202.3665 [astro-ph]. (Visited on 06/02/2025).
- Gardner, Jonathan P. et al. (June 2023). "The James Webb Space Telescope Mission". In: *Publications of the Astronomical Society of the Pacific* 135, p. 068001. ISSN: 0004-6280. DOI: 10.1088/1538-3873/acd1b5. (Visited on 05/30/2025).
- Gillon, Michael (Apr. 2024). "The Double Phase Curve of TRAPPIST-1b and c at 15 Microns". In: p. 9116. DOI: 10.5194/egusphere-egu24-9116. (Visited on 01/20/2025).
- Gillon, Michaël et al. (May 2016). "Temperate Earth-sized Planets Transiting a Nearby Ultracool Dwarf Star". In: *Nature* 533, pp. 221–224. ISSN: 0028-0836. DOI: 10.1038/nature17448. (Visited on 04/22/2025).
- Gillon, Michaël et al. (Feb. 2017). "Seven Temperate Terrestrial Planets around the Nearby Ultracool Dwarf Star TRAPPIST-1". In: *Nature* 542, pp. 456–460. ISSN: 0028-0836. DOI: 10.1038/nature21360. (Visited on 04/30/2025).

- Gommers, Ralf et al. (Jan. 2025). “Scipy/Scipy: SciPy 1.15.0”. In: *Zenodo*. DOI: 10.5281/zenodo.14593523. (Visited on 06/03/2025).
- Gordon, Karl D. et al. (Dec. 2024). “The James Webb Space Telescope Absolute Flux Calibration. II. Mid-infrared Instrument Imaging and Coronagraphy”. In: *The Astronomical Journal* 169.1, p. 6. ISSN: 1538-3881. DOI: 10.3847/1538-3881/ad8cd4. (Visited on 06/10/2025).
- Greene, Thomas P. et al. (June 2023). “Thermal Emission from the Earth-sized Exoplanet TRAPPIST-1 b Using JWST”. In: *Nature* 618, pp. 39–42. ISSN: 0028-0836. DOI: 10.1038/s41586-023-05951-7. (Visited on 01/20/2025).
- Grimm, Simon L. et al. (May 2018). “The Nature of the TRAPPIST-1 Exoplanets”. In: *Astronomy and Astrophysics* 613, A68. ISSN: 0004-6361. DOI: 10.1051/0004-6361/201732233. (Visited on 02/05/2025).
- Hastings, W. K. (Apr. 1970). “Monte Carlo Sampling Methods Using Markov Chains and Their Applications”. In: *Biometrika* 57.1, pp. 97–109. ISSN: 0006-3444. DOI: 10.1093/biomet/57.1.97. (Visited on 05/06/2025).
- Higson, Edward et al. (Sept. 2019). “Dynamic Nested Sampling: An Improved Algorithm for Parameter Estimation and Evidence Calculation”. In: *Statistics and Computing* 29.5, pp. 891–913. ISSN: 0960-3174, 1573-1375. DOI: 10.1007/s11222-018-9844-0. arXiv: 1704.03459 [stat]. (Visited on 06/03/2025).
- Ih, Jegug et al. (July 2023). “Constraining the Thickness of TRAPPIST-1 b’s Atmosphere from Its JWST Secondary Eclipse Observation at 15 Mm”. In: *The Astrophysical Journal Letters* 952.1, p. L4. ISSN: 2041-8205. DOI: 10.3847/2041-8213/ace03b. (Visited on 06/11/2025).
- Iyer, R. Aishwarya et al. (June 2022). *The SPHINX M-dwarf Spectral Grid. I. Benchmarking New Model Atmospheres to Derive Fundamental M-Dwarf Properties*. DOI: 10.5281/zenodo.7416042. (Visited on 05/13/2025).
- Luger, Rodrigo et al. (June 2017). “A Seven-Planet Resonant Chain in TRAPPIST-1”. In: *Nature Astronomy* 1, p. 0129. ISSN: 2397-3366. DOI: 10.1038/s41550-017-0129. (Visited on 01/13/2025).
- Mayor, Michel and Didier Queloz (Nov. 1995). “A Jupiter-mass Companion to a Solar-Type Star”. In: *Nature* 378.6555, pp. 355–359. ISSN: 1476-4687. DOI: 10.1038/378355a0. (Visited on 04/25/2025).
- Perryman, Michael (2018). *The Exoplanet Handbook*. 2nd ed. Cambridge: Cambridge University Press. ISBN: 978-1-108-41977-2 978-1-108-30416-0.
- Rieke, G. H. et al. (July 2015). *The Mid-Infrared Instrument for the James Webb Space Telescope, I: Introduction*. Tech. rep., p. 1. (Visited on 05/30/2025).
- Turbet, Martin et al. (Apr. 2018). “Modeling Climate Diversity, Tidal Dynamics and the Fate of Volatiles on TRAPPIST-1 Planets”. In: *Astronomy & Astrophysics* 612, A86. ISSN: 0004-6361, 1432-0746. DOI: 10.1051/0004-6361/201731620. (Visited on 05/05/2025).
- Villanueva, G. L. et al. (Sept. 2018). “Planetary Spectrum Generator: An Accurate Online Radiative Transfer Suite for Atmospheres, Comets, Small Bodies and Exoplanets”. In: *Journal of Quantitative Spectroscopy and Radiative Transfer* 217, pp. 86–104. ISSN: 0022-4073. DOI: 10.1016/j.jqsrt.2018.05.023. (Visited on 06/16/2025).
- Winn, Joshua N. (Sept. 2014). *Transits and Occultations*. DOI: 10.48550/arXiv.1001.2010. arXiv: 1001.2010 [astro-ph]. (Visited on 03/12/2025).
- Zhang, Michael et al. (Oct. 2024). *Retrievals on NIRCam Transmission and Emission Spectra of HD 189733b with PLATON 6, a GPU Code for the JWST Era*. DOI: 10.48550/arXiv.2410.22398. arXiv: 2410.22398 [astro-ph]. (Visited on 06/16/2025).
- Zieba, Sebastian et al. (Aug. 2023). “No Thick Carbon Dioxide Atmosphere on the Rocky Exoplanet TRAPPIST-1 c”. In: *Nature* 620, pp. 746–749. ISSN: 0028-0836. DOI: 10.1038/s41586-023-06232-z. (Visited on 01/20/2025).

## A Appendix: Additional figures

This appendix gathers some additional figures that were not displayed in the Results section as they were not essential to the global comprehension of my work or redundant with others.

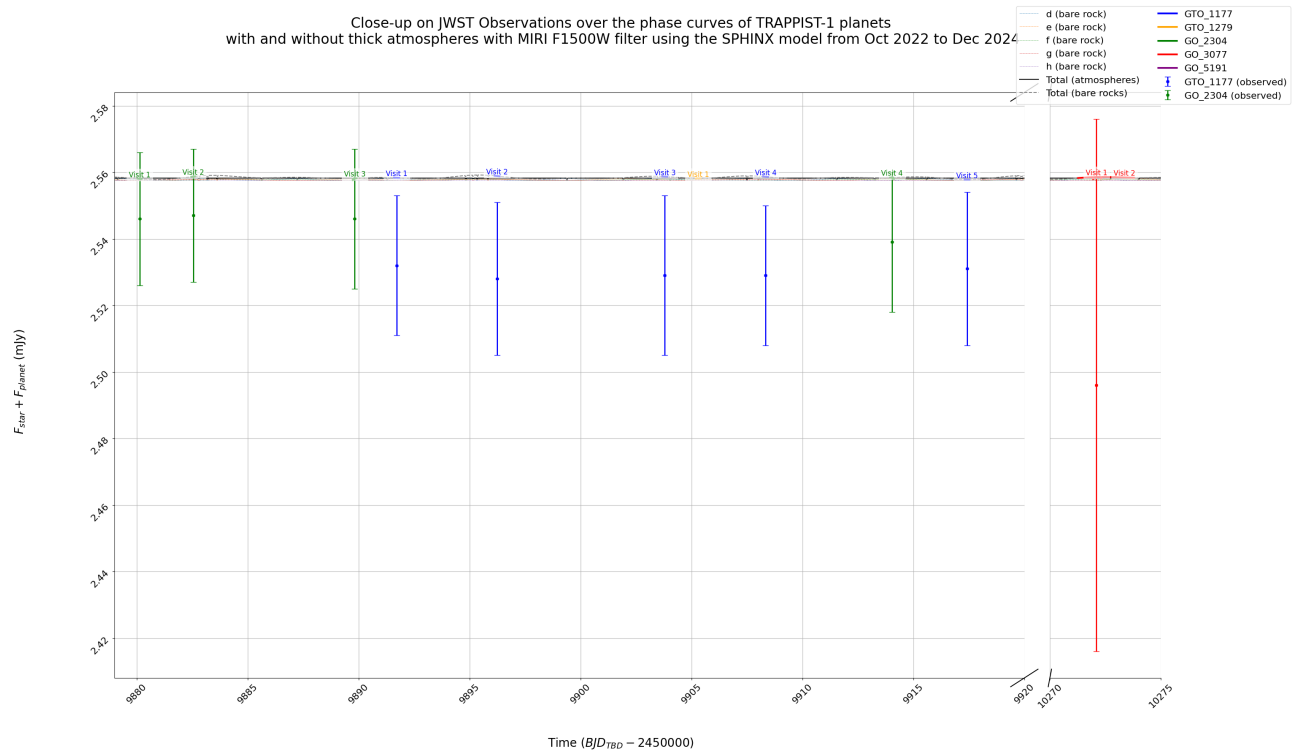


Figure 21: Comparison between the fluxes measured by the JWST and the simulated flux variations due to the outer planets of TRAPPIST-1 with the F1500W MIRI filter and the SPHINX model. There is no offset in the position of the data points. The error bars have been reduced to the optimistic case of a 1% error (Gordon et al. 2024) for the GTO 1177 and GO 2304 programs but the one for the GO 3077 phase curve is far more realistic.

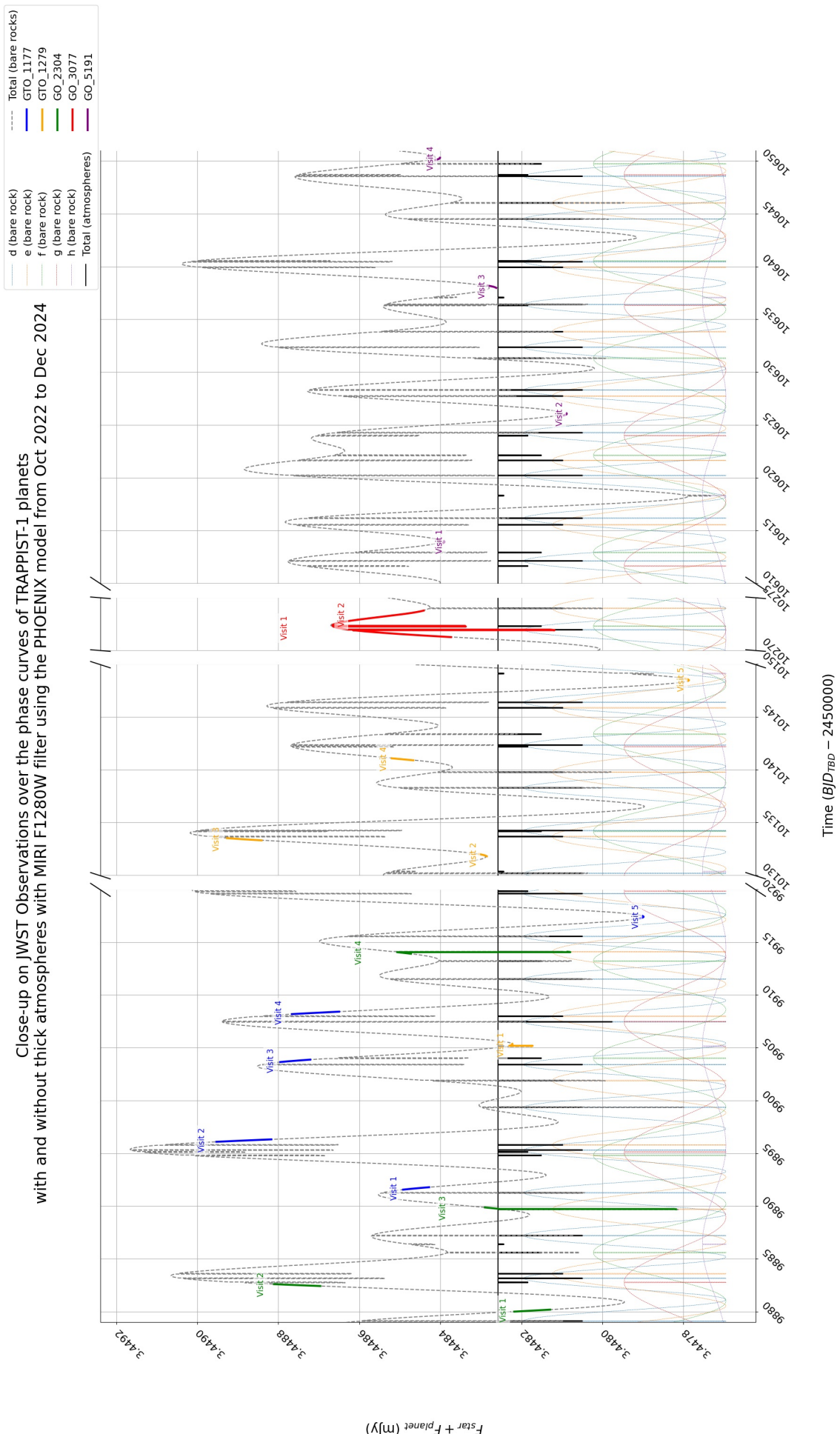


Figure 22: Simulation of the phase curves of the outer planets of TRAPPIST-1 in absolute fluxes using the PHOENIX model for the F1280W MIRI filter. Transits are not displayed for better readability. The JWST observations are displayed in color over the total curve for the bare rock case. The flux of each outer planet as a bare rock is displayed to show its phase over time.

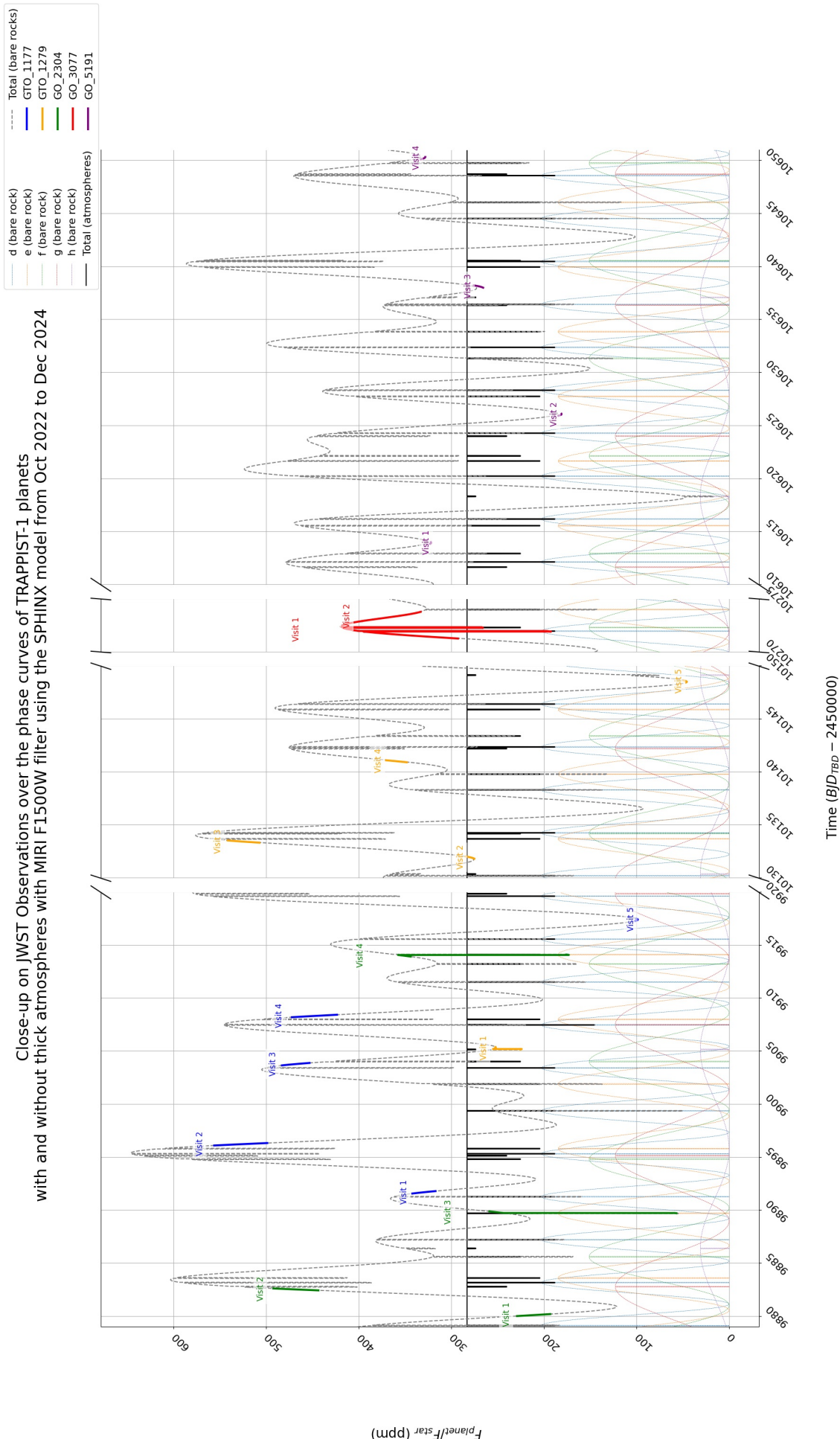


Figure 23: Simulation of the phase curves of the outer planets of TRAPPIST-1 in relative fluxes using the PHOENIX model for the F1500W MIRI filter. Transits are not displayed for better readability. The JWST observations are displayed in color over the total curve for the bare rock case. The flux of each outer planet as a bare rock is displayed to show its phase over time.

## B Appendix: Presentation of the Exoplanets\_Phase\_Curves codes

In this appendix, I will give more information about the Exoplanets\_Phase\_Curves Python codes that I wrote to simulate the phase curves of the TRAPPIST-1 planets. I plan to write a clean documentation in the future but in the mean time I will present the main codes of my simulations and the ones that the reader might need to run if he or she wants to reproduce the figures of Section 3 and Appendix A in order for example to be able to zoom into them. For better clarity, I will omit the all files that were only used for tests, that were not completed, that are redundant with others or that are outputs of other ones.

As explained before, I made my codes fully available on GitHub so that anyone can use it for his or her work or propose improvements. Thus, they can be downloaded at the following URL: [https://github.com/LJ-Cartigny/Exoplanets\\_Phase\\_Curves](https://github.com/LJ-Cartigny/Exoplanets_Phase_Curves).

To begin with, the `Solar_System_constants.py` file contains constants from the Solar System bodies, such as the Sun and Earth radii or masses, that are then used to express the values of the parameters of the TRAPPIST-1 star and planets in `TRAPPIST1_parameters.py`.

These parameters are used by the `Orbital_motion.py` code which contains all the functions that are necessary to compute a planet's true anomaly by solving the Kepler equation (Eq. 3) thanks to the `optimize.solve` function from the Scipy library ([Gommers et al. 2025](#)). The output is then used in the `Phase_curve_v1.py` file, which contains the first version of my codes to simulate a planet phase curve, with a bolometric flux, over a given period of time. It includes a function to use the Lambertian model of the phase curve (Eq. 14) for inclined and elliptical orbits and one with the sine model (Eq. 15) for non-inclined and circular orbits. For example, this code was used to generate Figure 11. To determine whether the planet is in an eclipse or not, this code uses the functions in `Transits.py`.

The `Phase_curve_TTV.py` file contains the functions to simulate the phase curves with the sine model for non-inclined and circular orbits using reference times for the transits. These functions are the ones that were used to compute my results in Sections 3.1.2 and 3.3.2 and the phase curves can be saved in .txt files. The transits predictions take the TTVs into account and are in the `Files_TTV` folder.

The functions in the `Flux_wavelength.py` are used to compute the fluxes observed by the different MIRI filters using either the SPHINX, PHOENIX or black body spectra, the bandpasses of the MIRI filters being in the `miri_filter.csv` file which was provided by my supervisors. This code also contains functions to compute a planet's equilibrium temperature and to convert fluxes from  $\text{W/m}^2/\text{m}$  to mJy and vice-versa. It was used to make the comparison in Figure 18.

The `JWST_Obs_simu.py` contains a function used to compute the phase curves of the planets of TRAPPIST-1 during the JWST observations and save them in .txt files.

The `JWST_Obs_plot.py` file is the one to run if the reader wants to reproduce figures of Sections 3.1.2 and 3.3.2 and of Appendix A to zoom into the plots or just plot other cases. This code uses the functions of the previous ones to simulate a phase curve between the first JWST observation in Table 3 and the last one and place them in color over the total curve. The user can change several parameters at the beginning of the code to for example select which planets he or she wants to plot, with which MIRI filter and which stellar spectrum model (SPHINX or PHOENIX). He or she can also choose if the curve will use relative fluxes in ppm or absolute fluxes in mJy. It is also possible to choose whether to plot the data points from JWST observations or not for the specified filter and if an offset will be used to place the points at the same level than the curves (like in Figure 19). Finally, if the phase curve for a given set of planets, with a given filter and a given spectrum model has already been computed, it is possible to specify to not do the simulation again in order to save some time.

## C Appendix: Observations with JWST

In Table 4, I give more information about the JWST observations with MIRI of eclipses of TRAPPIST-1 b and c from which I used data during my internship with exact values of the data points in Figures 19 and 21. The targets and references for each observation are already in Table 3.

Program ID	Visit	Start time (UTC)	End time (UTC)	Filter	Observed flux (mJy)
GTO 1177	1	2022-11-08 02:17:33	2022-11-08 07:47:10	F1500W	$2.532 \pm 0.021$
GTO 1177	2	2022-11-12 15:05:09	2022-11-12 20:34:15	F1500W	$2.528 \pm 0.023$
GTO 1177	3	2022-11-20 04:24:30	2022-11-20 09:54:11	F1500W	$2.529 \pm 0.024$
GTO 1177	4	2022-11-24 17:26:22	2022-11-24 23:00:44	F1500W	$2.529 \pm 0.021$
GTO 1177	5	2022-12-03 19:25:56	2022-12-04 00:37:36	F1500W	$2.531 \pm 0.023$
GTO 1279	1	2022-11-21 16:39:04	2022-11-21 21:46:11	F1280W	$3.725 \pm 0.031^a$
GTO 1279	2	2023-07-06 08:13:36	2023-07-06 13:12:41	F1280W	$3.425 \pm 0.020$
GTO 1279	3	2023-07-07 20:27:41	2023-07-08 01:28:53	F1280W	$3.428 \pm 0.019$
GTO 1279	4	2023-07-15 10:31:31	2023-07-15 15:02:53	F1280W	$3.427 \pm 0.018$
GTO 1279	5	2023-07-22 23:02:40	2023-07-23 04:03:14	F1280W	$3.428 \pm 0.020$
GO 2304	1	2022-10-27 12:55:21	2022-10-27 17:22:35	F1500W	$2.546 \pm 0.020$
GO 2304	2	2022-10-29 23:03:01	2022-10-30 03:22:25	F1500W	$2.547 \pm 0.020$
GO 2304	3	2022-11-06 05:42:51	2022-11-06 09:45:53	F1500W	$2.546 \pm 0.021$
GO 2304	4	2022-11-30 10:43:10	2022-11-30 15:03:50	F1500W	$2.539 \pm 0.021$
GO 3077	1	2023-11-22 18:33:39	2023-11-24 10:13:19	F1500W	$2.496 \pm 0.08$
GO 3077	2	2023-11-24 10:13:23	2023-11-25 06:55:41	F1500W	no value
GO 5191	1	2024-10-30 08:46:02	2024-10-30 12:35:46	F1280W	$3.416 \pm 0.016$
GO 5191	2	2024-11-11 10:45:26	2024-11-11 15:14:22	F1280W	$3.412 \pm 0.016$
GO 5191	3	2024-11-23 12:39:00	2024-11-23 17:53:24	F1280W	$3.403 \pm 0.020$
GO 5191	4	2024-12-05 15:25:26	2024-12-05 20:31:59	F1280W	$3.380 \pm 0.016$

Table 4: Complementary information about the JWST observations of TRAPPIST-1 b and c eclipses with MIRI. <sup>a</sup>: This value was not plotted in my plots for the reasons explained below.

The observed fluxes were measured at the moment when the planet is totally occulted by the star so that the values only contain the flux from the star and the other planets.

The value from visit 1 of GTO 1279 ([Ducrot et al. 2024b](#)) was not shown in Figures 19 and 21 because for this visit, the observation team tried to place the star TRAPPIST-1 in the bottom-right corner of the detector in order to include another star in the array that could be used for systematic corrections. However, there was no gain from this comparison star and the detector turned out to be more noisy (in particular the flat field) in the bottom-right corner of the array. Consequently, the PIs of the program ask to replace the star at the center of the detector for the 4 remaining visits, as it was the case for programs GTO 1177 and GO 3077. This is why the value of this visit has been discarded.

We also note that GO 3077 ([Gillon 2024](#)) is divided in 2 visits but that there were both consecutive. This splitting in two visits arises from a technical limit with JWST for long continuous stares (here the full observations last almost 60 hours).